

E-ISSN: 2709-9423 P-ISSN: 2709-9415 Impact Factor (RJIF): 5.29 JRC 2025; 6(2): 182-200 © 2025 JRC

Received: 29-07-2025 Accepted: 30-08-2025

Mohammad M Al-Tufah Directorate of Education, Kirkuk, Ministry of Education.

Anaam Khalif Al-Azzawy, Department of Education, Salah Al-Din Education Directorate, Tikrit, Iraq

Diaa M Najim
Department of Education,
Kirkuk Education Directorate,
Kirkuk, Iraq

Synthesis, characterization, and theoretical (DFT) analysis of new schiff bases derived from 4-aminoantipyrin for molecular docking and biological activity

Mohammad M Al-Tufah, Anaam Khalif Al-Azzawy and Diaa M Najim

DOI: https://www.doi.org/10.22271/reschem.2025.v6.i2c.224

Abstract

Schiff bases have important applications in biological activities and combating harmful bacteria, so they are important in the medical and pharmaceutical aspects. They can be synthesized from the reaction of compounds containing carbonyl groups (aldehydes and ketones) with compounds containing a free amine group (primary amines). In this research, new Schiff base derivatives were prepared through addition and condensation reactions by adding 4-aminoantipyrene to substituted aromatic aldehydes (2,4-dichlorobenzaldehyde and 4-methoxybenzaldehyde) and substituted aromatic ketones (acetophenone and 2-hydroxyacetophenone) in addition to sulfanilic acid. The catalyst was glacial acetic acid, and ethanol was used as a solvent. The prepared compounds were characterized by FT-IR spectroscopy. ¹H-NMR and ¹³C-NMR were used to characterize the structures of some of them. In addition, mass spectrometry was used to verify the successful preparation of compounds A₁ and A₂. The biological activity of the prepared compounds A₁, A₄, and A₅ was studied against two types of bacteria: Gram-negative (Klebsiella) and Gram-positive (Staphylococcus aureus and Enterococcus faecalis). The compounds showed broad activity at high concentrations (0.01, 0.001 mg/ml), while the activity of these compounds decreased at high concentrations. To understand the biological activity of compounds A₁ and A₄, molecular docking was studied, and the results showed that the binding strength of these compounds to the active site of the protein is (-7.86, -7.63 Kcal/mol) compared to the standard compound (-8.62 Kcal/mol). To determine the electronic properties of the prepared compounds, the density-to-energy-band theory (DFT) was used, and it was found that compound A₁ has the smallest energy gap among the compounds. The distribution of partial charges of the prepared compounds was also measured.

Keywords: 4-Aminoantypirin, Schiff base, biological activity, molecular docking

Introduction

Heterocycles comprise almost half of all known organic compounds, making them one of the most important chemical classes. Heterocycles containing nitrogen are essential components for the production of pharmaceuticals. Pyrazoles are a type of heterocyclic compounds that include nitrogen and are thought to be especially important bioactive systems. Knorr's first successful synthesis of a pyrazolone-derived molecule was antipyrine [1-3]. The chemistry of antipyrine compounds has attracted a lot of attention in materials science and health due to their prospective uses as analgesics, antipyretics, and non-steroidal anti-inflammatory medications [4, 5]. 4 -Aminoantipyrine, a derivative of antipyrine, amino antipyrine, possesses a variety of biological goings-on, as well as antibacterial, antiviral, and analgesic properties. Due to It is readily accessibile free amino group, it is also used to create metal complexes. This group id=s utilized to react with phenols or carbonyl compounds (aldehyde or ketone) to form azo or azomethine molecules [6]. Although 4-Aminoantipyrine (4-AAP) (Figure 1) is an anti-inflammatory, its use as nonsteroidal anti-inflammatory drugs is rare because it can cause agranulocytosis, a decrease in the number of infection-fighting white blood cells [7]. Many research groups have expressed interest in the synthesis of 4-aminoantipyrine derivatives due of their potential biological activity. In this regard, a wide rang of bioactivities, including analgesic [8], anti-inflammatory [9], antibacterial [10], and anticancer goings-on [11], have been documented for 4-aminoantipyrine derivatives and their metal complexes. Our interested in the antibacterial, as significant bacterial infections have become increasingly resistant to antibiotics over the past ten years. Furthermore, emerging and re-

Correspondence
Mohammad M Al-Tufah
Directorate of Education,
Kirkuk, Ministry of Education.
Iraq

emerging bacterial infectious diseases continue to cause morbidity and mortality worldwide. [12]. Schiff bases, commonly referred to as imines or azomethines, are chemical compounds that were initially identified by Hugo Schiff. They are produced when primary amines condense with aldehydes or ketones [13]. 4-AAP, or aminoantipyrine A five-membered pyrazolone ring with two nitrogen atoms, a double bond, an imine (C=N), and a carbonyl group (C=O) makes up the intriguing family of chemical compounds known as Schiff base derivatives. Because of their easy production, these compounds have attracted a lot of attention from researchers. Condensing the main amine group of 4-AAP with the carbonyl group of different aldehydes or ketones makes them simple to make. They are

an interesting topic for chemical study, as this approach gives access to a broad range of compounds with high yields [14]. This research aims to contribute to the field of medicinal chemistry by synthesizing and characterizing novel Schiff base derivatives derived from 4-aminoantipyrine. The significance of this work extends beyond its theoretical contributions to include potential practical applications, as their biological activity will be evaluated alongside a study of their molecular docking and Density Functional Theoty (DFT). This work represents a significant step towards discovering compounds with potent biological activity and unique physical properties, thus inaugural new streets for the growth of innovative drugs and functional materials.

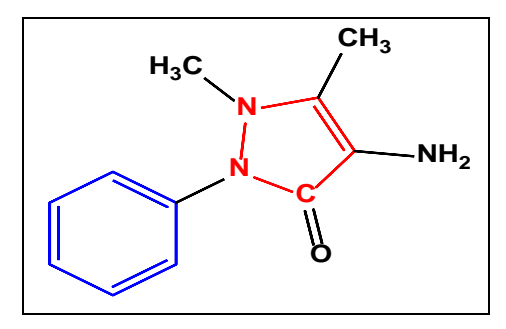


Fig 1: Structure of 4- Aminoantipyrine

Materials and Methods

The following substances were provided by Fluka-Aldrich without additional purification: utilized Aminoantipyrene, 2,4-dichlorobenzaldehyde, methoxybenzaldehyde, 2-hydroxyacetophenone, acetophenone, sulfanilic acid, ethanol, and glacial acetic acid. Compound melting points were measured using an uncorrected electrothermal melting point instrument. The Shimadzu FTIR-8400 spectrophotometer captured the FT-IR spectra on a KBr disk. Tetramethylsilane (TMS) was used as a standard to register 1HNMR and 13CNMR spectra on Bruker spectroscopic ultra-shield magnets 300 MHz devices. To ascertain the binding position of drugs within the protein active site, molecular docking experiments were conducted using AutoDock Vina. Using the B3LYP functional and the 3-21G bases set, density functional theory (DFT) computations using Gaussian 09W were used to assess the electronic and structural characteristics.

Preparation of Schiff bases Preparation of compound $[A_1 \text{ and } A_2]^{[15]}$

4-aminoantipyrine (2 g, 0.01 mol) and substituted benzaldehydes (0.01 mol) were dissolved in 40 ml of absolute ethanol. A small quantity of glacial acetic acid was added. The mixture was refluxed for 3 hours at 80 °C while stirring. After cooling to room temperature, the reaction

mixture was put over crushed ice and stirred. The precipitate was then filtered, dried, and refined by recrystallization from ethanol. Table 1 displays the physical properties of compounds $(A_1 \text{ and } A_2)$.

Preparation of compound [A₃ and A₄] [16].

Compound 4-aminoantipyrine (4 g, 0.02 mol) and substituted acetophenone (0.02 mol) in absolute ethanol (30 ml) were mixed, and 2 ml of glacial acetic acid was added. The mixture was refluxed for 4-5 hours at 80 $^{\circ}$ C with stirring. The reaction mixture was agitated and poured over crushed ice after it had cooled to room temperature. The resulting precipitate was then filtered, dried, and crystallized from acetone. Table 1 illustrates the physical properties of compounds (A₃ and A₄).

Preparation of compound [A₅].

Sulfanilic acid (1.73 g, 0.01 mol) was dissolved in a flask with a round bottom with 50 ml of water. 4-aminoantipyrine (2 g, 0.01 mol) was added dropwise from a dropping funnel. After three hours of heating at $100 \,^{\circ}\text{C}$ in a water bath, the mixture was chilled for half an hour in an ice bath. Filtration was used to remove the precipitate, which was then recrystallized from ethanol. Table 1 displays the compound (A_5) physical characteristics.

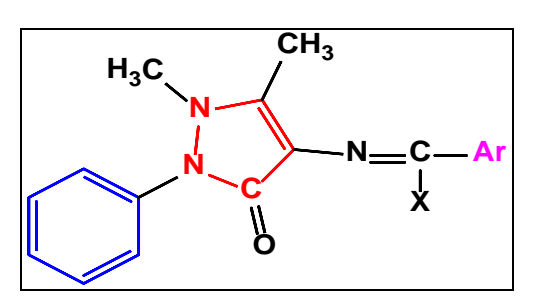


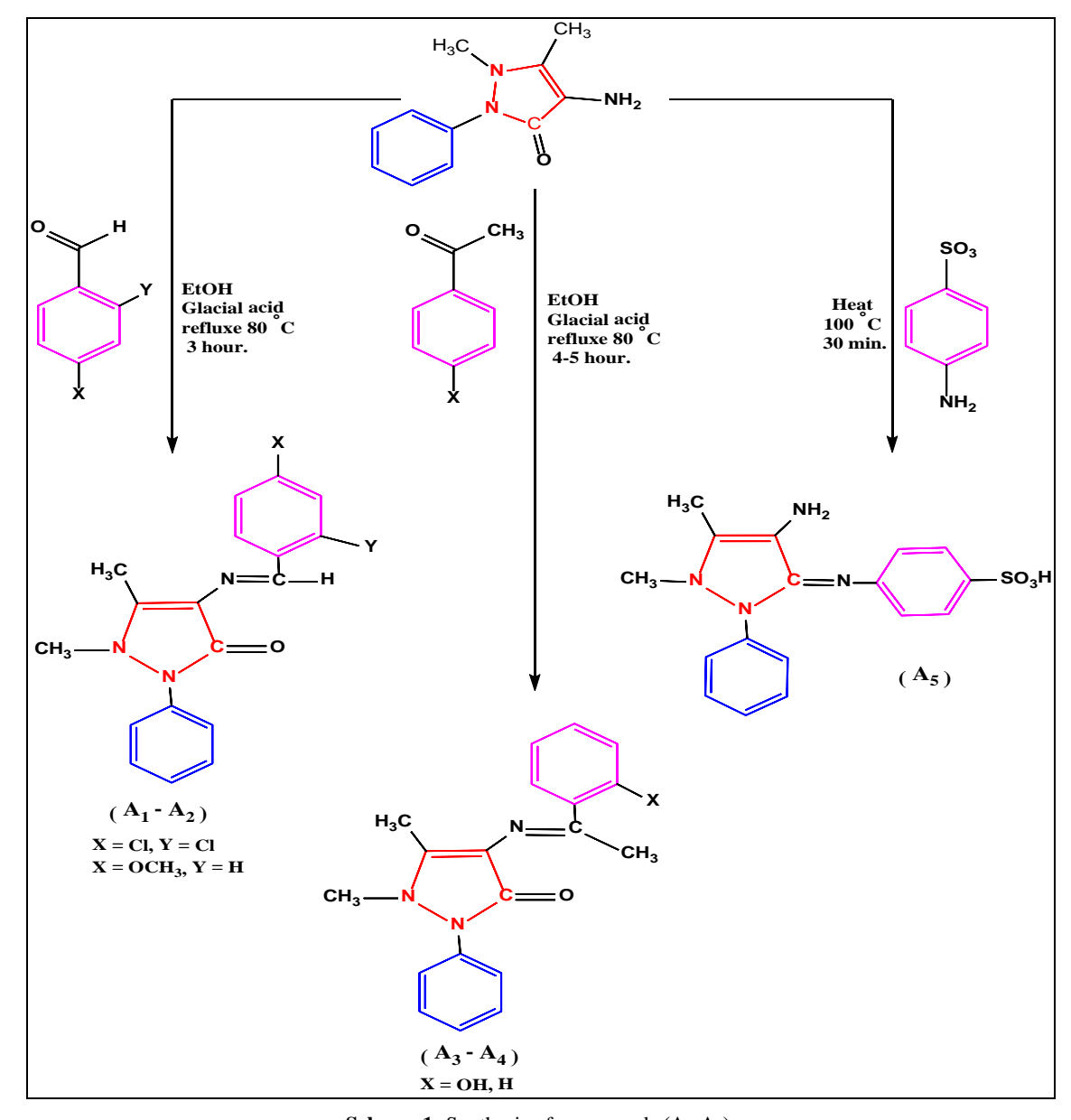
Fig 2: General structure of 1, 3, 4-oxadiazole derivatives substituted with aryl and imine functional groups

Table 1: shows	some physical	properties of	compounds	$(A_1 - A_5)$.

Compound No.	Ar	X	Molecular Formula	Color	M.P °C	Yield %
\mathbf{A}_1	cı -cı	Н	$C_{18}H_{15}Cl_2N_3O$	Orang	212-214	84
\mathbf{A}_2	≥och₃	Н	$C_{19}H_{19}N_3O_2$	Yellow	227-229	81
\mathbf{A}_3	⊰ —⟨⟩	CH ₃	$C_{19}H_{19}N_3O$	Brown	224-226	83
A ₄	₹ HO	CH ₃	$C_{19}H_{19}N_3O_2$	Red	217-219	80
A ₅	ζ so₃H	Н	$C_{17}H_{18}N_5O_3S$	White Off	108-110	86

Results and Discussion: The synthesis of the compounds A_1 - A_5 was produced through the reaction of 4-aminoantypyirin with substituted aldehydes, substituted acetophenone, and sulfanilic acid in ethanol, The process

included a nucleophilic attack by the amine group on the carbonyl carbon, resulting in unstable which formed an intermediate. This intermediate subsequently eliminated a water molecule to yield an imine [17], as seen in Scheme 1.



Scheme 1: Synthesis of compounds (A_1-A_5) .

Spectroscopic interpretation FT-IR

The compound A₁ FT-IR spectra, which is displayed in Figure 2, was examined. The elimination of the distinctive absorption bands for the carbonyl (C=O) group of the aldehyde group at 1730 cm⁻¹ and the main amine (NH₂) group of 4-aminoantipyirine at 3425 cm⁻¹ was a significant discovery [18]. The successful construction of the Schiff bases was verified at the same time by the emergence of many new bands. Strong absorption bands at 1633 cm⁻¹, which are indicative of the newly generated azomethine (C=N) functional group [19], were most prominently detected. Additionally, absorptions were detected at 1558-1548 cm⁻¹, 1652 cm⁻¹, and 3042 cm⁻¹. υ(C-H) for the aromatic ring, v(C=O) for the pyrazolone ring, and v(C=C)for the aromatic ring are represented by these absorptions, respectively. The Schiff base compound A₂ FT-IR spectra, which is displayed in Figure 3, was examined. At 3058 cm⁻¹, 1652 cm⁻¹, 1616 cm⁻¹, and 1600-1551 cm⁻¹, peaks were seen. The stretching vibrations of the pyrazolone ring's C=O bond [20], the aromatic C-H bond, the azomethine C=N bond, and the aromatic ring's C=C bond are attributed to

these peaks, respectively. Figure 4 displays the analysis of the Schiff base compound A₃ FT-IR spectrum. At 3116 cm⁻¹, 1627 cm⁻¹, and 1576 cm⁻¹, peaks were seen. These peaks are attributed to the stretching vibrations of the azomethine C=N bond, the aromatic C-H link, and the C=O bond of the pyrazolone ring, respectively [21]. The Schiff base compound A₄ FT-IR spectra, which is displayed in Figure 5, was investigated. 3323 cm⁻¹, 2983, 2882 cm⁻¹, 1662 cm⁻¹, and 1575 cm⁻¹ were the identified peaks. The stretching vibrations of the (OH) group, the aromatic C-H bond, the C=O bond of the pyrazolone ring, and the azomethine C=N bond belong to these peaks, respectively. Figure 6 displays the analysis of the Schiff base compound A₅ FT-IR spectrum. The following peak locations were noted: 3458 cm⁻¹, 3056 cm⁻¹, 1630 cm⁻¹, 1618 cm⁻¹, and 1600,1561 cm-1. The stretching vibrations of the (NH2) group, the aromatic C-H bond, the azomethine C=N bond, the olefinic (C=C), and the aromatic C-H bond are attributed to these peaks, respectively. Table 2 displays the remaining absorptions.

Table 2: FT-IR Compounds Spectrum Data (A₁-A₅)

Compound No.	υ (C-H) Aromatic	υ (C=O) pyrazolone	υ (C=N) imine	υ (C=C) Aromatic (Sym., Asy.)	Other absorptions
A_1	3042	1652	1633	1558, 1485	υ (C-Cl) 769 cm ⁻¹
A_2	3058	1652	1616	1600, 1551	υ (C-O) 769 cm ⁻¹
A ₃	3116	1627	1576	1533, 1445	υ (C-N) 1381-1148 cm ⁻¹
A_4	3044	1662	1575	153, 1456	υ (O-H) 3323 cm ⁻¹
A_5	3056	-	1630	1600, 1561	υ (SO ₃) 1155, 1021 cm ⁻¹

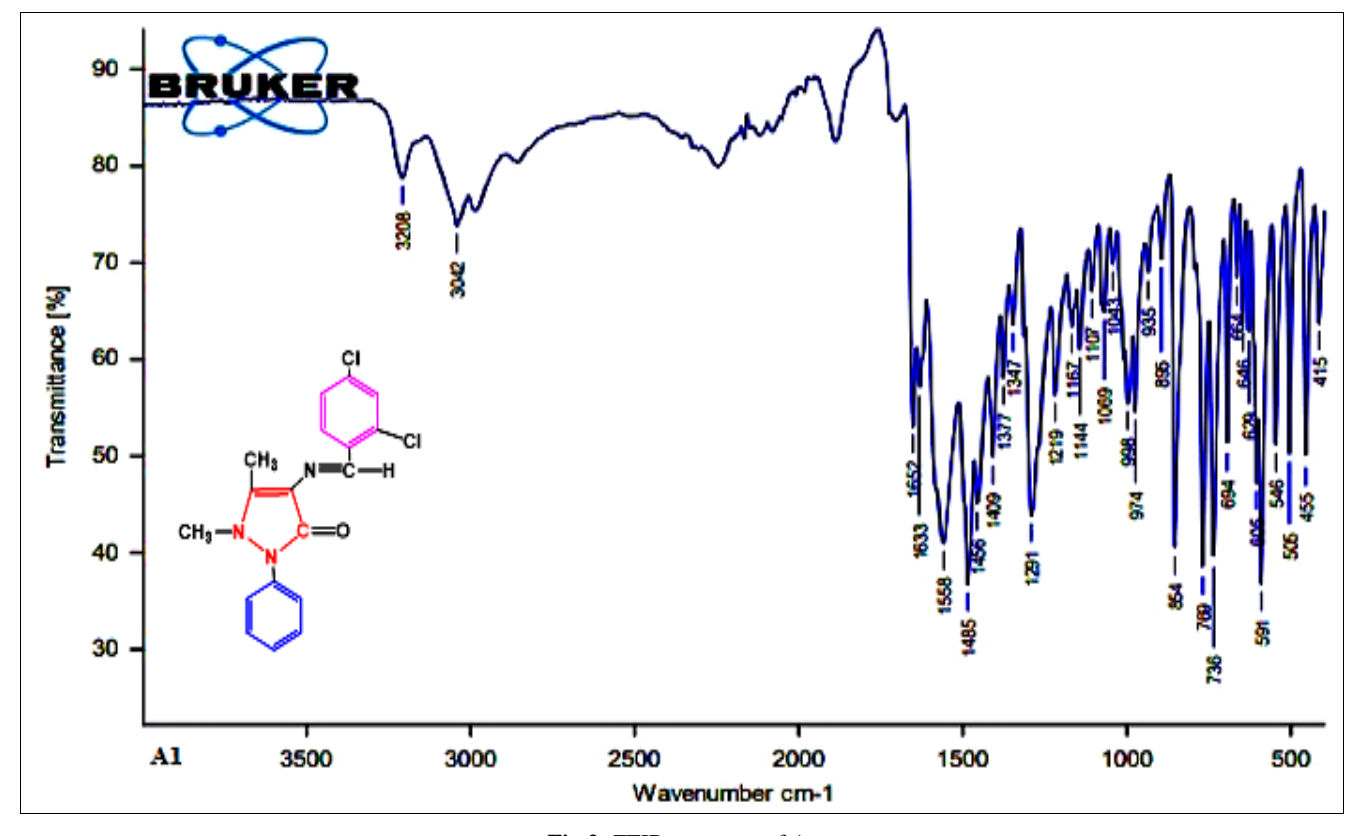


Fig 2: FTIR spectrum of A₁

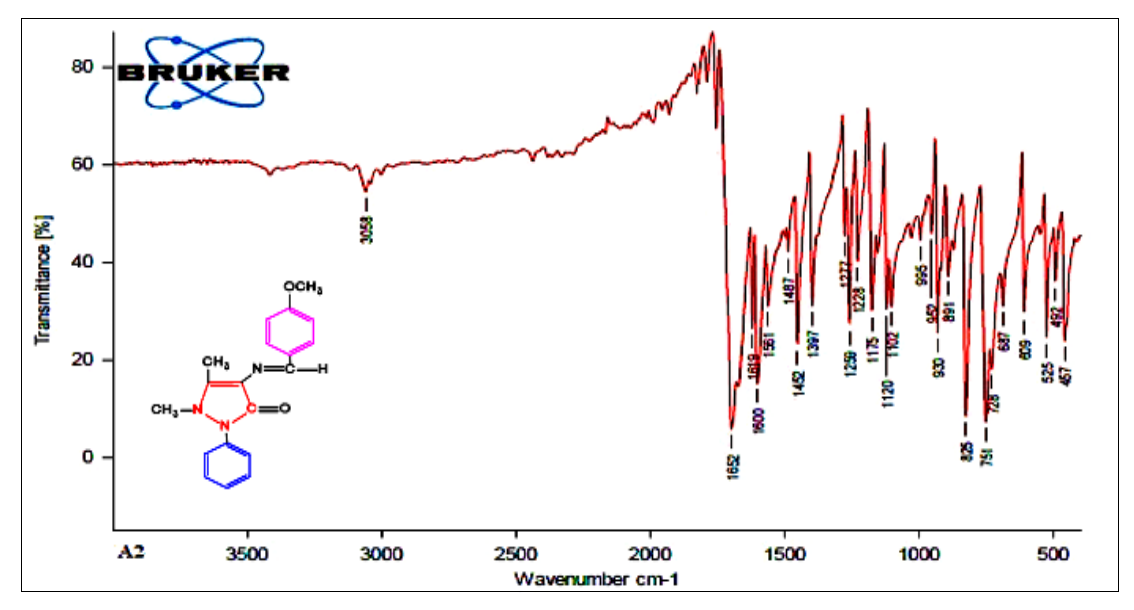


Fig 3: FTIR spectrum of A_2

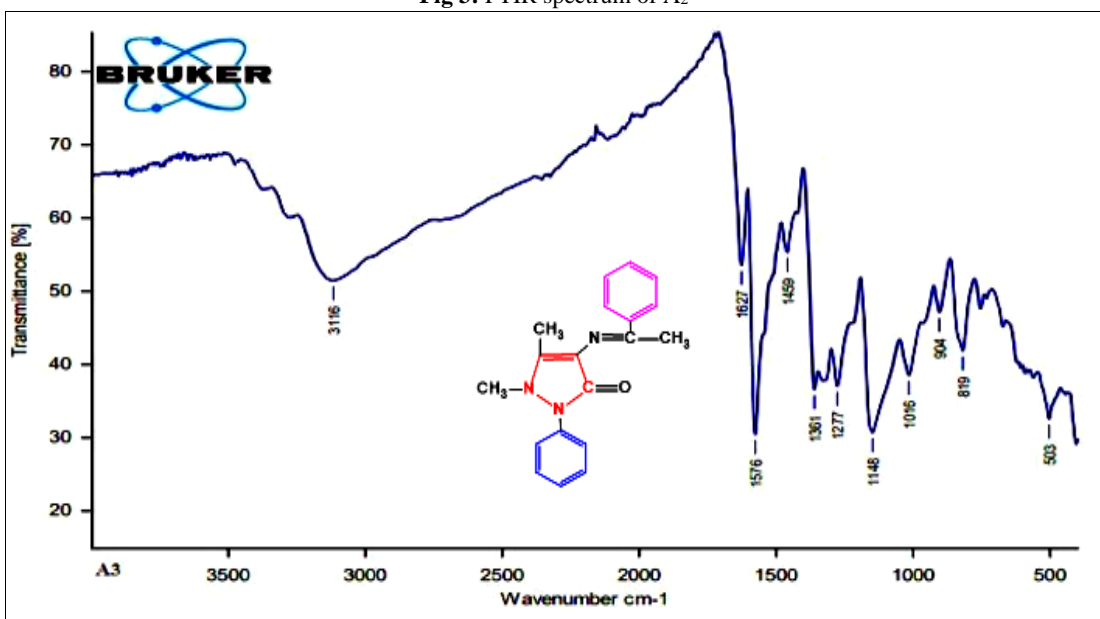


Fig 4: FTIR spectrum of A₃

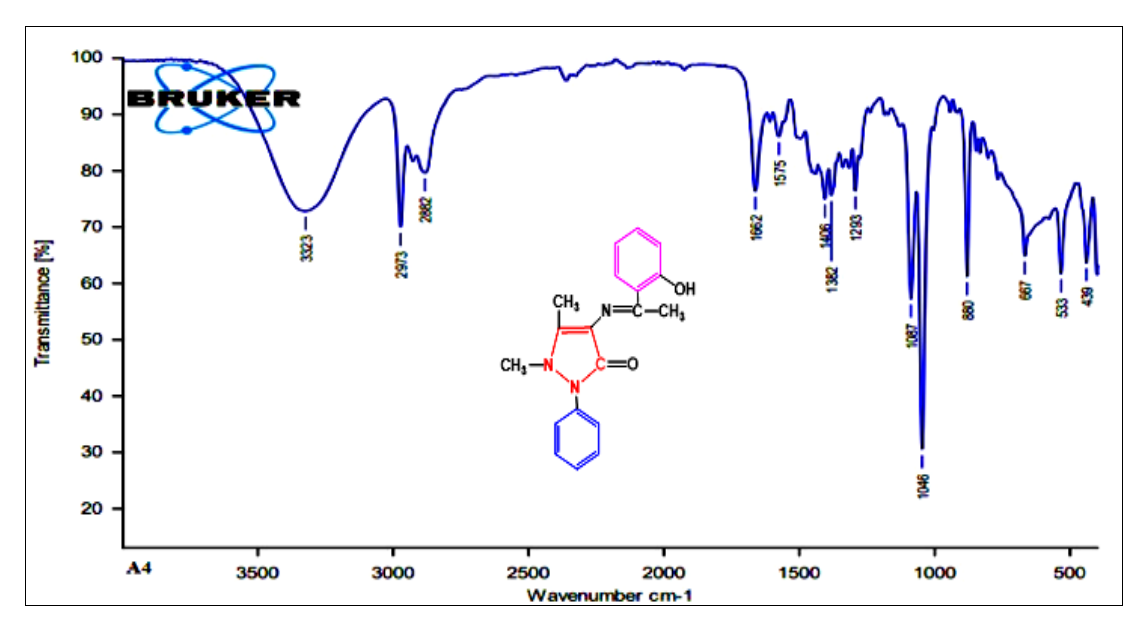


Fig 5: FTIR spectrum of A₄

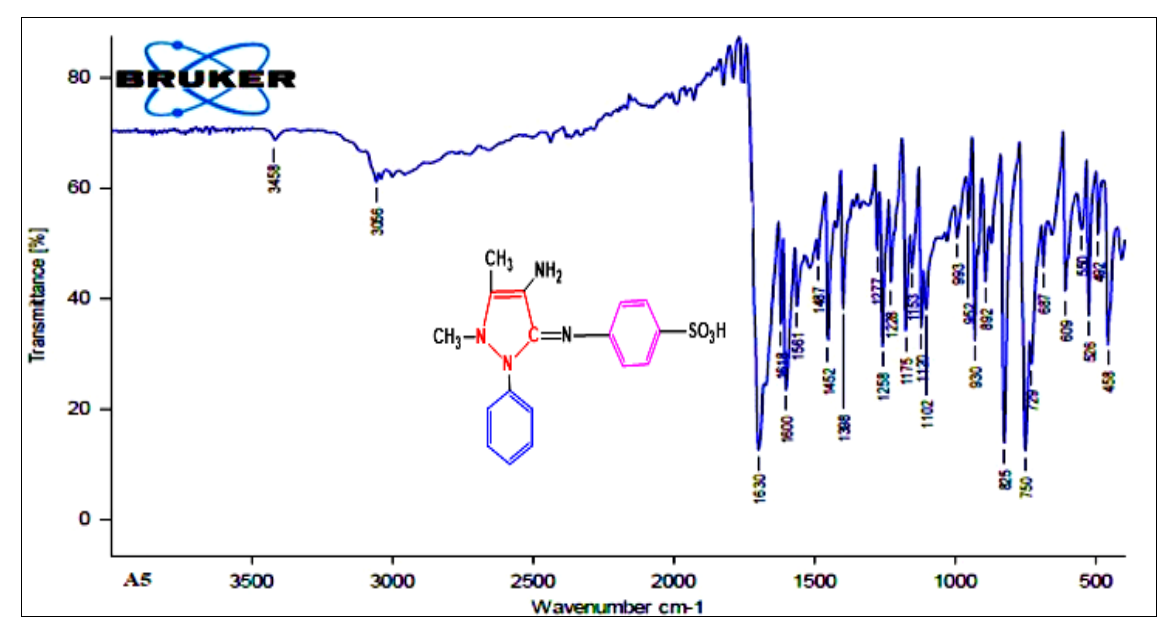


Fig 6: FTIR spectrum of A

Spectroscopic interpretation ¹H-NMR and ¹³C-NMR.

The (¹H-NMR) spectrum of the compound A₁ in Figure 7 reveals a singlet signal at 2.73 ppm related to the three protons of a methyl group (3H, CH₃), a singlet signal at 3.37 ppm generated by the three protons of a methyl group connected to a nitrogen atom (3H, CH₃-N) ^[22]. The eight protons of two aromatic rings (8H, Ar-H) produce a multiplet signal at 6.92-8.65 ppm, while the proton of an imine group generates a singlet signal at 9.65 ppm.

Figure 8 shows the (1H-NMR) band of compound A₂, which exhibits a singlet signal at 3.03 ppm owing to the three protons of a methoxy group (3H, OCH₃) and a singlet signal at 4.71 ppm created by the three protons of a methyl group (3H, CH₃). The protons of two aromatic rings (9H, Ar-H) produce a multiplet signal at 6.99-7.91 ppm, while the proton of an imine group gives a singlet signal at 9.31 ppm [²³].

The (1H-NMR) spectra for compound A₃ in Figure 9 indicates, the three protons of a methyl group attached to an imine (3H, CH₃-C=N) produce a singlet signal at 1.95 ppm, the three protons of a methyl group attached to a nitrogen atom (3H, CH₃-N) create a singlet signal at 4.25 ppm, and the three protons of a methyl group attached to a nitrogen atom (3H, CH₃-N) give a singlet signal at 5.73 ppm, and a multiplet signal at 6.20-7.52 ppm because of the two aromatic rings' eight protons (10H, Ar-H).

Figure up protons attached to the pyrazolone ring (3H, CH₃-C), a singlet signal at 3.5 ppm induced by three methyl group protons connected to the pyrazolone ring (3H, CH₃-N), and a singlet signal at 4.79 ppm induced by three amine group protons (2H, NH₂), a singlet signal at 8.48 ppm resulting from the proton of the hydroxyl group (1H, OH) and a multiplet signal at 7.21-7.46 ppm given by the protons of two aromatic rings (9H, Ar-H).

Figure 11 shows the 13C-NM spectrum of compound A_2 . The spectrum showed a signal due to the methyl carbon CH_3

at 22.6 ppm, a signal at 37.3 ppm due to the methyl carbon attached to the nitrogen (CH₃-N), and a signal at 56 ppm due to the methoxy carbon (OCH₃). The spectrum also showed a signal at 114 ppm due to the carbon pyrazolone ring (C-N). The aromatic system carbon showed signals at 116-144 ppm. The spectrum showed a signal at 154 ppm due to the carbon of the pyrazolone ring attached to the methyl group (C-CH₃), and signals at 156 ppm and 163 ppm due to the carbonyl carbon (C=O) and the carbon of the imine group (C=N), respectively.

The ¹³C-NMR spectrum of compound A₃ showed a signal at 30 ppm due to the methyl carbon (CH₃-C=N) and a signal at 33.9 ppm due to the carbon (CH₃-N). The carbon of the prazolone ring showed a signal at 113 ppm, signals at 116-137 ppm were due to the carbon of the aromatic ring, and signals at 145 ppm and 158 ppm were due to the carbonyl carbon (C=O) and the carbon of the azomethine group (C=N), respectively. See Figure 12.

Figure 13 shows the ¹³C-NMR spectrum of compound A₄. The spectrum showed several signals: a signal at 30.78 ppm belonging to the methyl group carbon (CH₃), a signal at 33 ppm belonging to the carbon (C=C) within the pyrazolone ring, a signal at 66.48 ppm belonging to the carbon (CH₃-N=C), and a signal at 113 ppm belonging to the carbon of the pyrazolone ring (C-N). As for the aromatic system carbon atoms, signals appeared at 116-137 ppm. A signal at 145 ppm also appeared, belonging to the carbonyl carbon (C=O), and a signal at 158 ppm belonged to the carbon of the imine group (C=N).

The 13 C-NMR spectrum of compound A_5 shown in Figure 14 showed a signal at 30 ppm due to the carbon of the methyl group (CH₃) and a signal at 66.448 ppm due to the carbon (CH₃-N). The spectrum showed multiple signals at 113-154 ppm due to the carbon of the aromatic system. A signal also appeared at 158 ppm due to the carbon of the azomethine group (C=N).

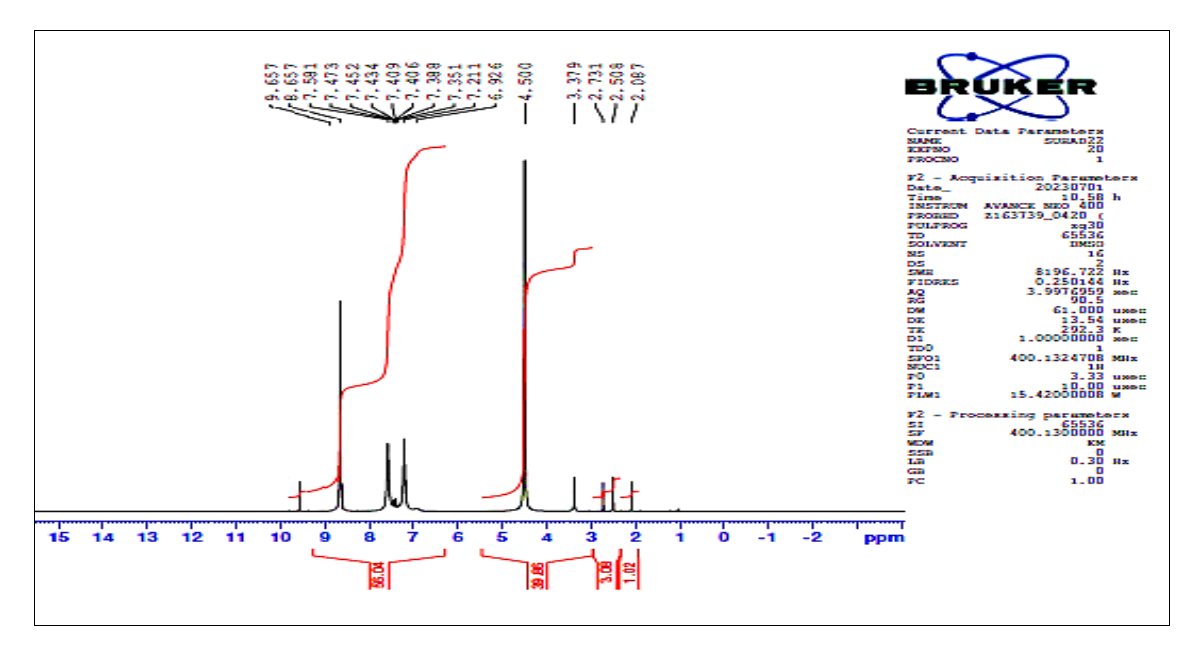


Fig 7: 1H-NMR spectrum of A₁

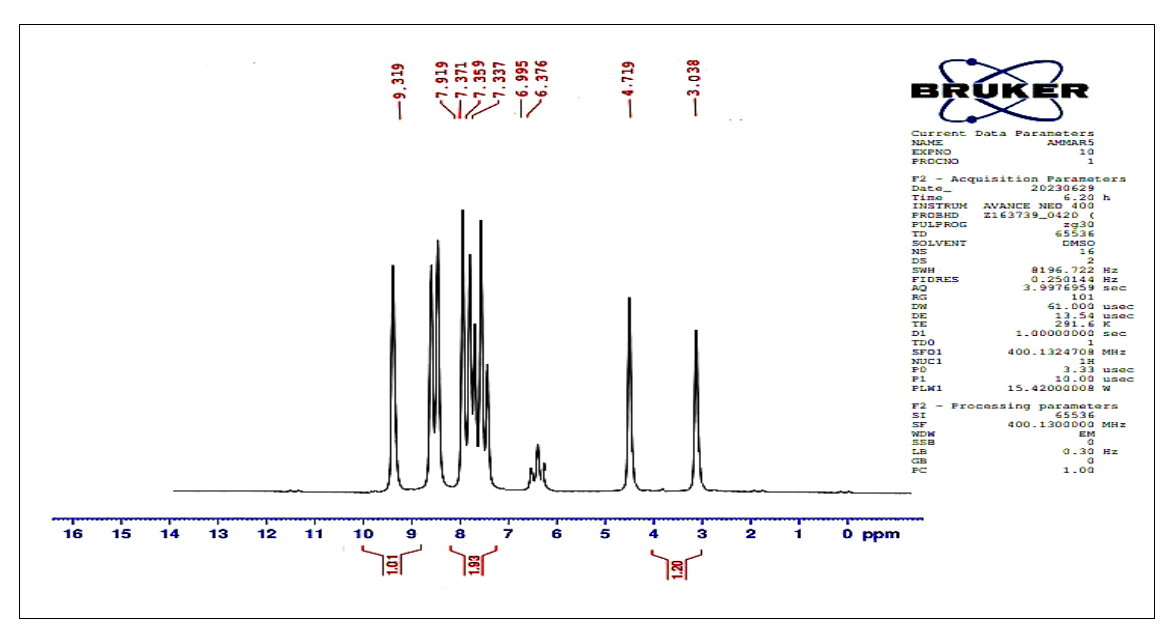


Fig 8: 1H-NMR spectrum of A₂

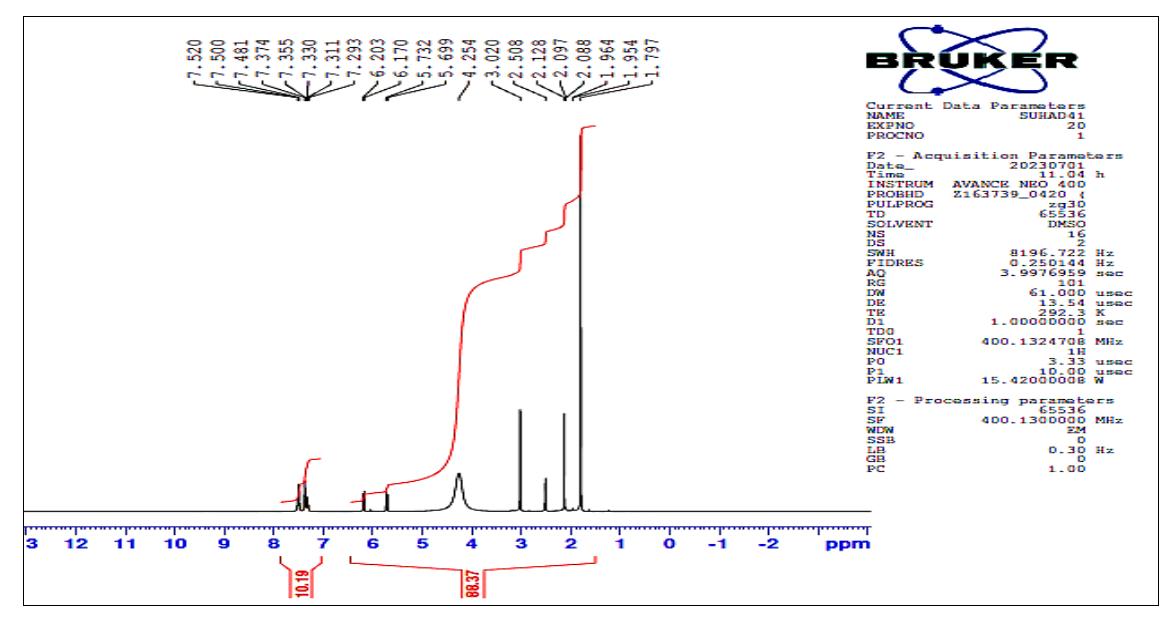


Fig 9: 1H-NMR spectrum of A₃

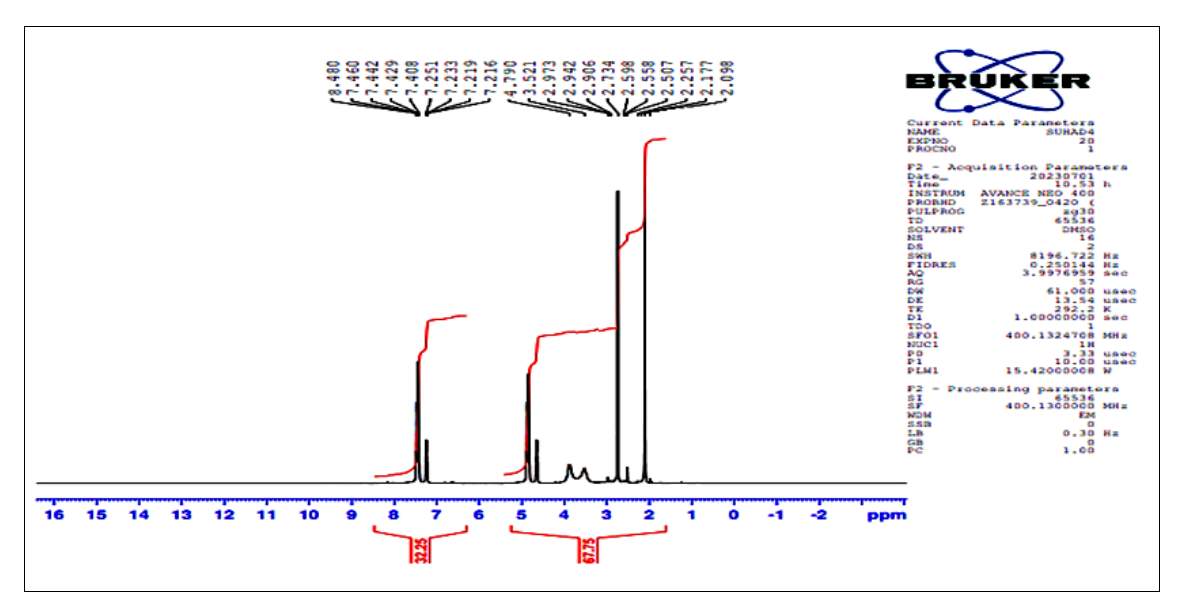


Fig 10: ¹H-NMR spectrum of A

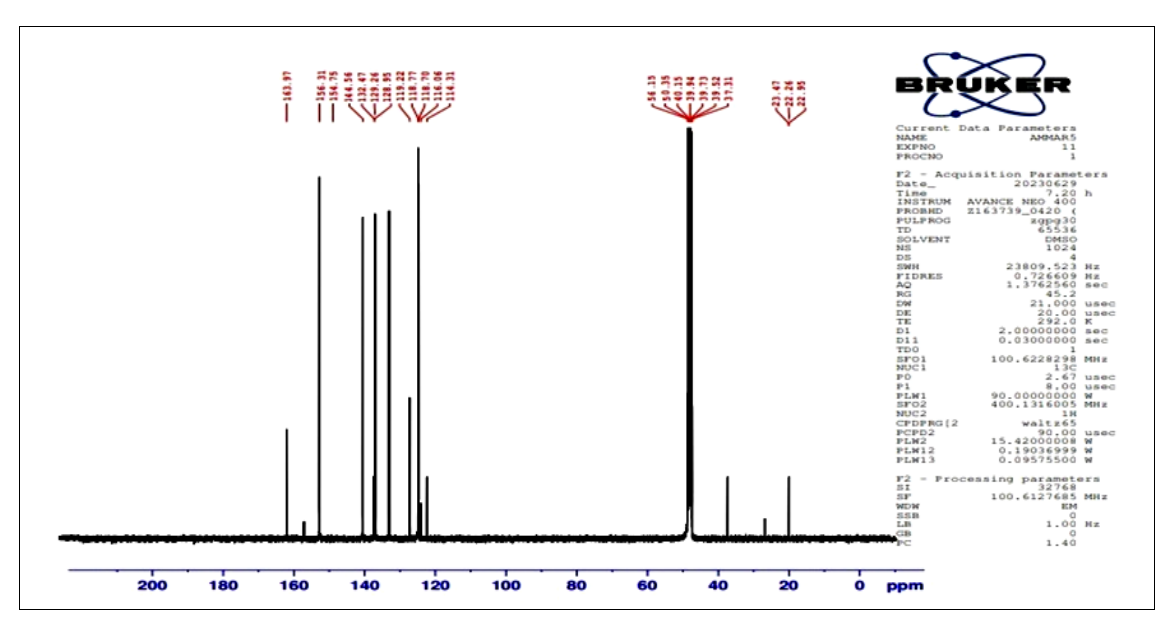


Fig 11: ¹³C-NMR spectrum of A₂

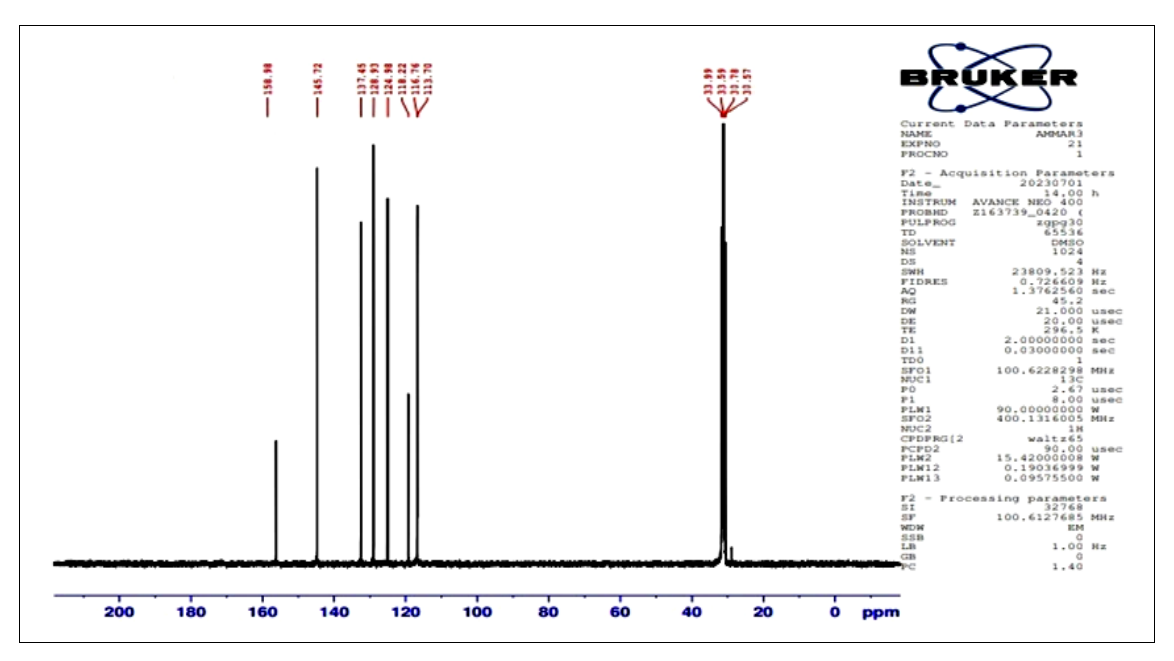


Fig 12: ¹³C-NMR spectrum of A₃

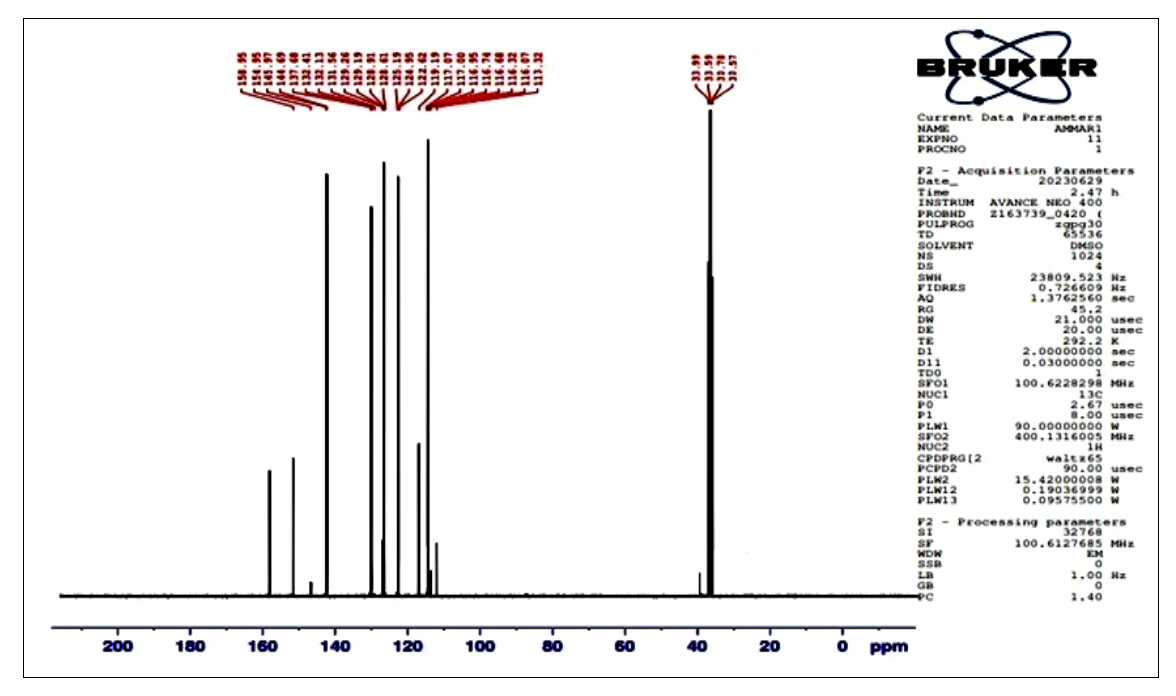


Fig 13: ¹³C-NMR spectrum of A₄

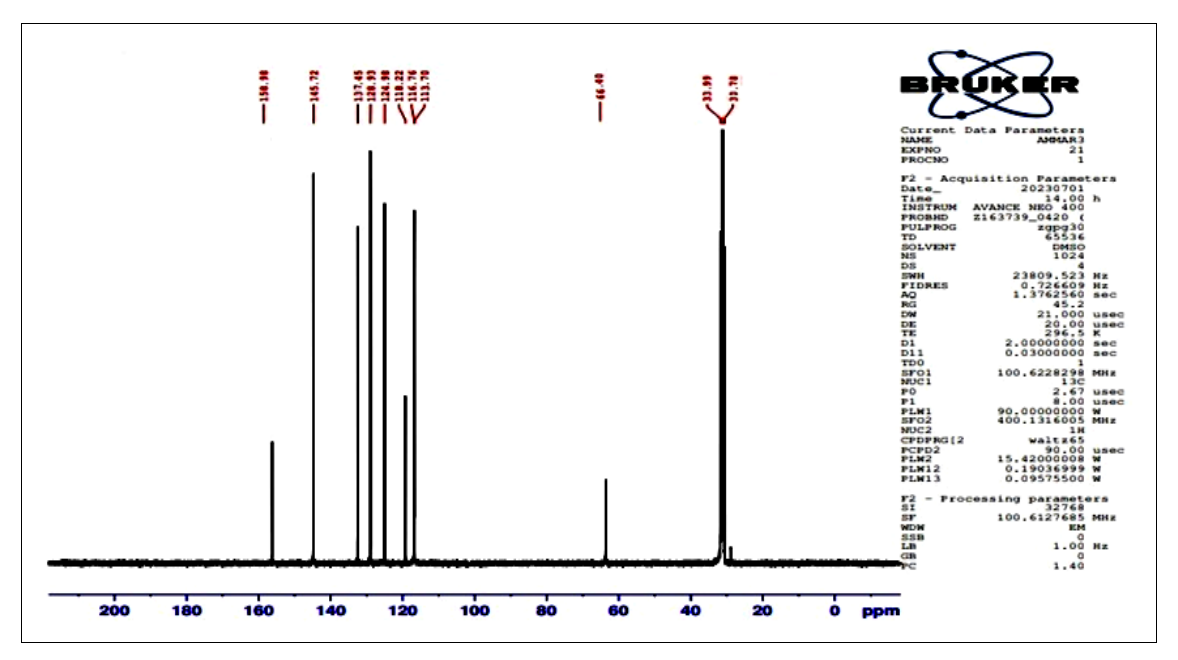


Fig 14: ¹³C-NMR spectrum of A₅

Mass spectral fragmentation pattern study of Compounds A_1 and A_2 .

Mass spectrometry results for both compounds A₁ and A₂ provide crucial insights into their chemical structures and molecular properties. This analytical technique works by measuring the mass-to-charge ratio (m/q) of ions formed when the compounds are fragmented [24]. The molecular ion peak in compound A₁'s mass spectrometry is located at m/q = 359.3, which is near the monoisotopic mass of 360.24 Da that is theoretically determined for the chemical formula [C₁₈H₁₅Cl₂N₃O]. There are two chlorine atoms in this formula, Cl. The natural abundance of the isotopes 35Cl and 37Cl is probably the cause of the observed small mass discrepancy, which creates a characteristic isotopic pattern. The base peak of the spectrum is found at m/q = 188.1, corresponding to the most stable fragment

[C₁₁H₁₂N₂O]⁺. This fragment is formed in the highest abundance. The other fragment peaks in the spectrum provide a fragmentation pathway, illustrating the step-bystep loss of specific chemical groups, including those containing chlorine atoms. This fragmentation pattern is vital for deducing the complete molecular structure. Mass spectrometry analysis of compound A2 revealed a molecular ion peak at m/q = 321.3, which is in excellent agreement with the theoretically calculated monoisotopic mass of 321.38 Da. This confirms the chemical formula as $[C_{19}H_{19}N_3O_2]$. The spectrum's base peak, located at m/q = 92.8, represents the most abundant and stable fragment ion, [C₆H₆ N]⁺. The other peaks in the spectrum correspond to the sequential fragmentation of the parent molecule, where different chemical groups are lost, providing key structural information. Note Table 3 and Figures 15 and 16.

Table 3: Mass spectrometry Fragmentation Peaks of Compounds A_1 and A_2 .

	Compound	$\overline{\mathbf{A}_1}$	Compound A ₂				
m/q	Chemical Formula	Peak Type	m/q	Chemical Formula	Peak Type		
359.3	$[C_{18}H_{15}Cl_2N_3O]$	Molecular Ion Peak	321	$[C_{19}H_{19}N_3O_2]$	Molecular Ion Peak		
314.1	$[C_{17}H_{17}ClN_3O]^{+\bullet}$	Fragment Peak	306.1	$[C_{18}H_{16}N_3O]^{+\bullet}$	Fragment Ion		
301.1	$[C_{16}H_{16}ClN_3O]^{+\bullet}$	Fragment Peak	281.1	$[C_{17}H_{18}N_3O]^{+\bullet}$	Fragment Peak		
275.1	$[C_{14}H_{14}ClN_3O]^{+\bullet}$	Fragment Peak	267.1	[C ₁₆ H ₁₇ N ₃ O] +•	Fragment Peak		
241.2	[C ₁₄ H ₁₅ N ₃ O] +•	Fragment Peak	255.2	[C ₁₅ H ₁₇ N ₃ O] +•	Fragment Peak		
215.1	[C ₁₂ H ₁₃ N ₃ O] +•	Fragment Peak	229.2	[C ₁₃ H ₁₅ N ₃ O] +•	Fragment Peak		
203.1	[C12H13N3O] +•	Fragment Peak	203.0	$[C_{11}H_{13}N_3O]^{+\bullet}$	Fragment Peak		
188.1	[C ₁₁ H ₁₂ N ₂ O] +•	Base peak	188.8	$[C_{11}H_{12}N_2O]^{+\bullet}$	Fragment Peak		
161.1	$[C_{10}H_{13}N_2]$	Fragment Peak	162.1	$[C_{10}H_{14}N_2]^{+\bullet}$	Fragment Peak		
122.0	$[C_7H_{10}N_2]$	Fragment Peak	148.9	$[C_9H_{11}N_2]^{+\bullet}$	Fragment Peak		
106.0	$[C_6H_6N_2]^{+\bullet}$	Fragment Peak	121.2	$[C_7H_9N_2]^{+\bullet}$	Fragment Peak		
77.0	[C ₆ H ₅] +•	Fragment Peak	107.0	$[C_6H_7N_2]^{+\bullet}$,	Fragment Peak		
57.9	$[C_4H_6]$	Fragment Peak	108.0	[C ₇ H ₈ O] +•	Fragment Peak		
			92.8	$[C_6H_6N]^{+\bullet}$	Base Peak		
			54.9	[C ₄ H ₆] +•	Fragment Peak		

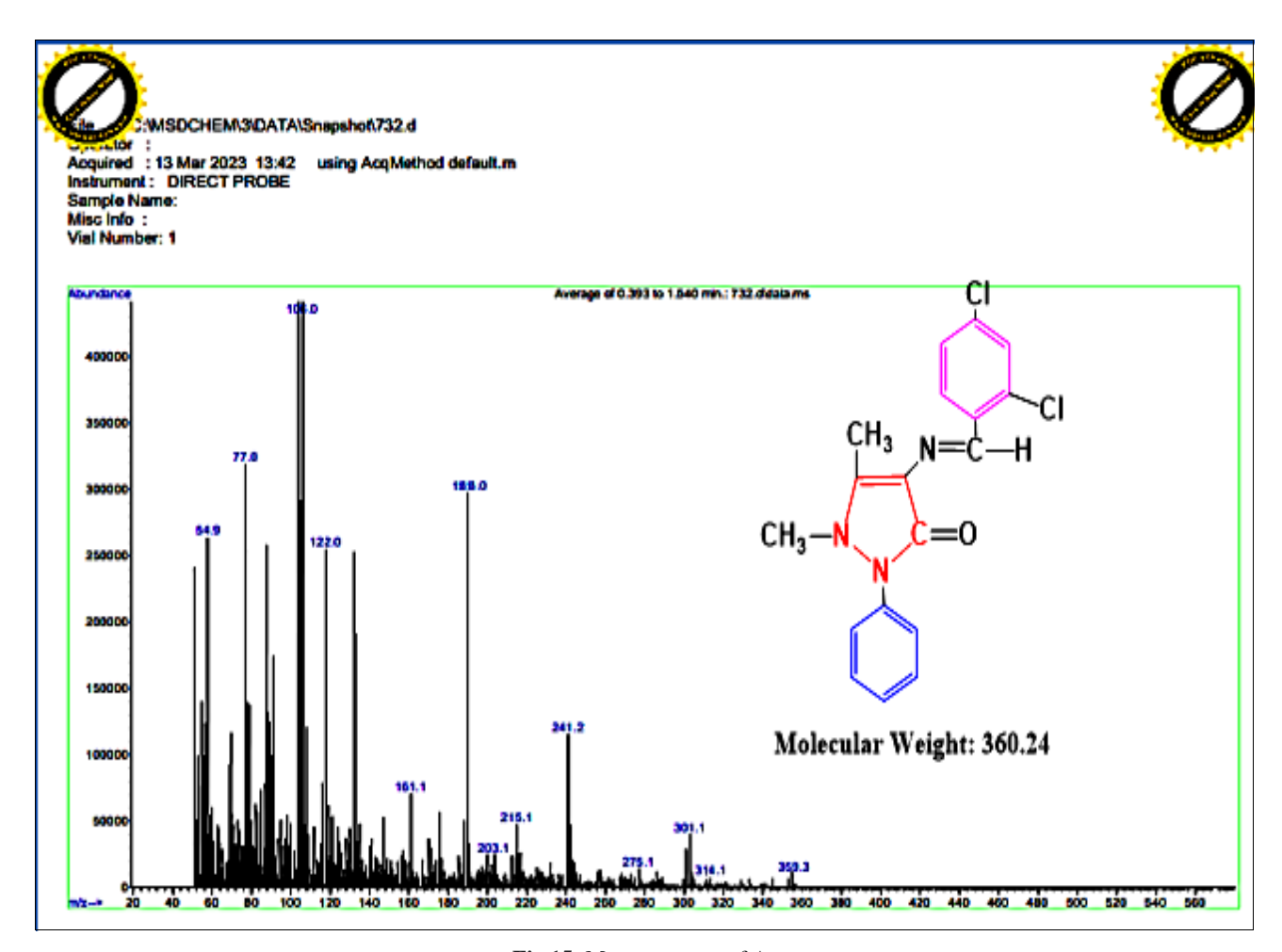


Fig 15: Mass spectrum of A_1

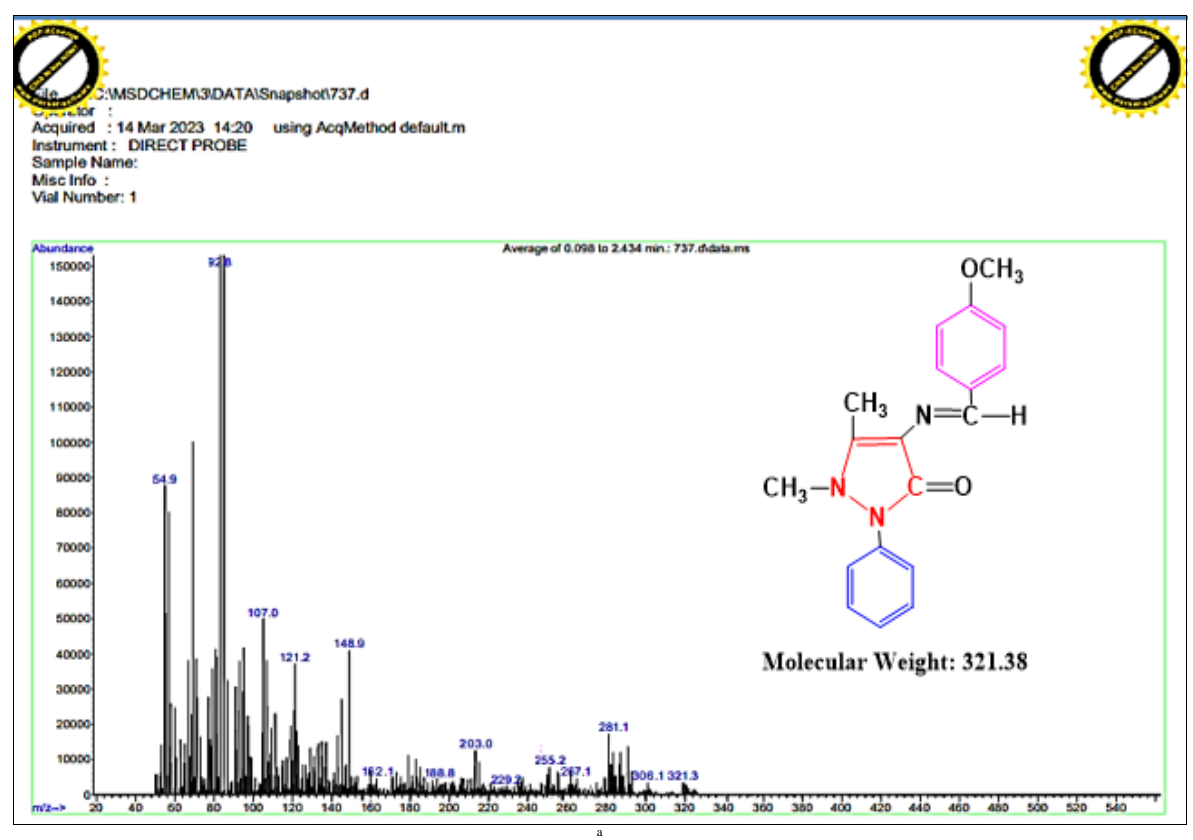


Fig 16: Mass spectrum of A2

Biological activity of some prepared compounds

The escalating threat of antimicrobial resistance is one of the most critical challenges facing global public health today [25]. This urgent crisis has intensified scientific efforts to discover and develop new compounds with potent antimicrobial activity. This study was designed to evaluate the antibacterial efficacy of three promising compounds $(A_1,$ A₄, and A₅) against a panel of clinically significant bacteria. Both the Gram-negative bacteria Klebsiella and the Grampositive pathogens Enterococcus faecalis Staphylococcus aureus were among the target species. To study the effect of the compounds on bacterial growth, the agar diffusion method was used at concentrations of (0.01, 0.001 and 0.0001 mg/ml) [26, 27]. The compounds showed a clear effect on bacterial growth at high concentrations.

Compound A₄ showed significant inhibitory activity against Klebsiella and Staphylococcus aureus bacteria; at the highest concentration of 0.01 mg/ml, the inhibition zone diameter reached 26 mm and 22 mm, respectively, at the highest. The inhibition zone diameter significantly at lower concentrations. With an inhibitory zone diameter of 24 mm, compound A₁ likewise showed considerable activity against Enterococcus faecalis; at lower doses, its efficacy also decreased. In contrast, Compound A5 was least effective against Klebsiella among the compounds tested, with a 14 mm inhibition zone diameter at maximum concentration. By increasing the diameter of the inhibition zone, it is clear that the effectiveness of the compounds against these types of bacteria increases at high concentrations. See Figures 17, 18, and 19.

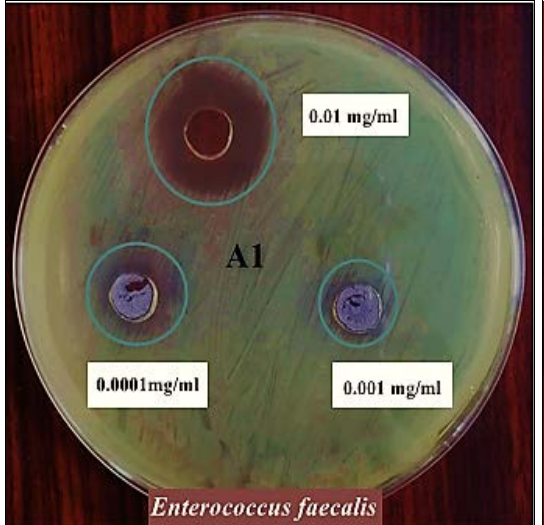


Fig 17 (a): Efficacy of Compound A₁ inhibiting the growth of *E. faecalis* bacteria.

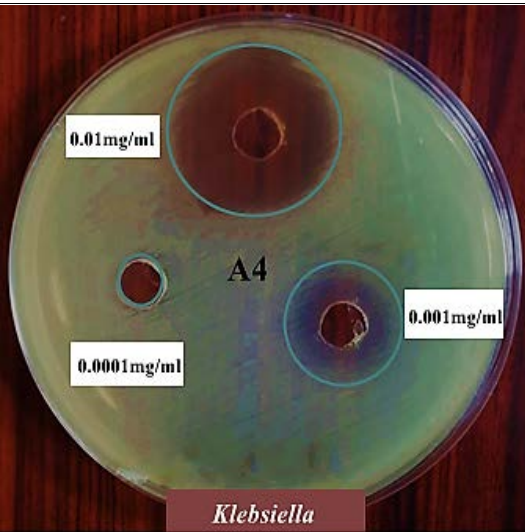
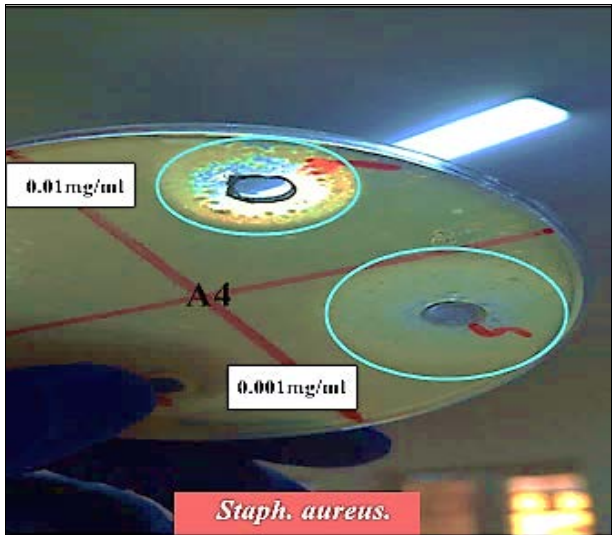


Fig 17 (b): Efficacy of Compound A₄ inhibiting the growth of *Klebsiella* bacteria.



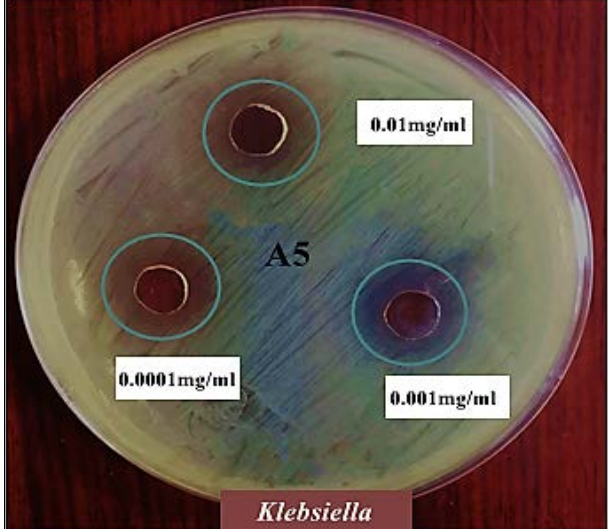


Fig 18(a): Efficacy of Compound A₄ inhibiting the growth of *Staph. aureus* bacteria.

Fig 18 (b): Efficacy of Compound A₄ inhibiting the growth of *Staph. aureus* bacteria.

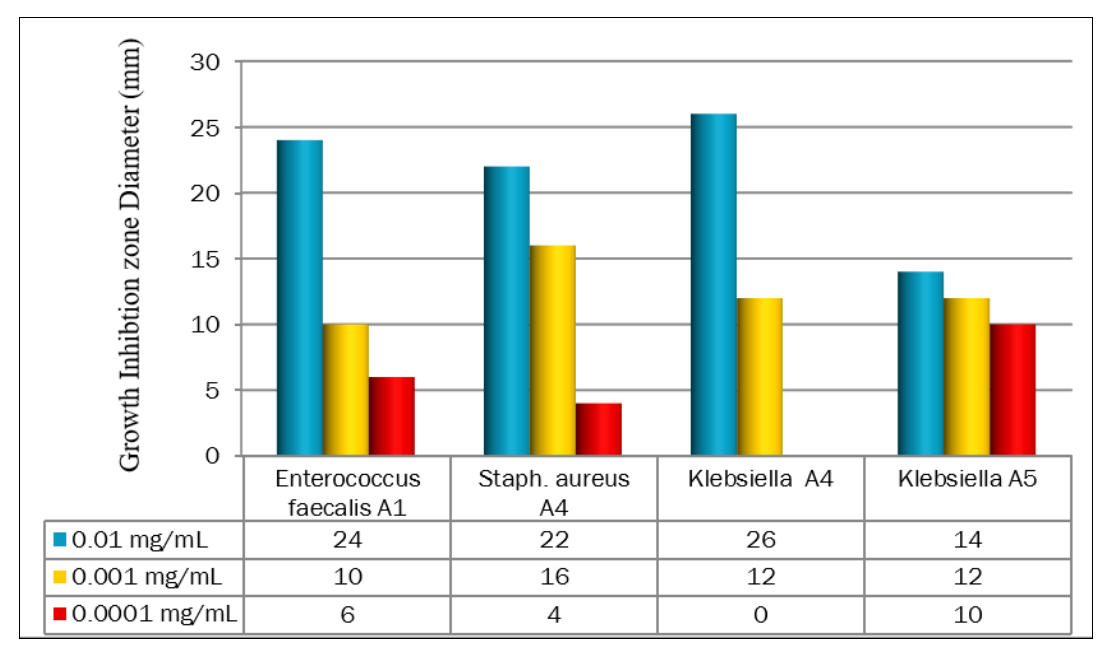


Fig 19: Antimicrobial Efficacy of Comparative A₁, A₄, and A₅ against Select Pathogens.

Docking studies

The newly synthesized compounds (A₁, A₄) were characterized for use in a molecular docking process. Their 3D structures generated using Chemdraw software and peroptimized with the AM and DFT method to ensure stability. To investigate their binding affinity, the optimized structures were then merged into a database using Molecular Operating Environment (MOE) software [28]. The protein Data Bank (PDB) provided the crystal structures of the proteins (8C7Y) [29]. In order to enable hydrogen bonding with the ligand, a water molecule was inserted into the active sites to prepare the structure. Hydrogen atoms were added to the structure and missing bonds were fixed [30]. The program (MOE, 2015) was used for all docking and scoring computations. The Protein Data Bank (PDB) provided the protein (8C7Y) crystal structure, which has a resolution of 1.65 Å. For dockin investigations, which often need for a resolution between 1.4 to 2.5 Å, this is regarded as a good resolution [31].

Results

One essential technique in the drug development process is molecular docking. MOE software was used in this investigation to forecast how the produced compounds A₁ and A₄ will bind to the target protein 8C7Y. The compound showed good binding affinity, and the nature of their interactions of key amino acide residuse in the protein was analyzed. The results revealed various types of interactions hydrogen bonding and hydrophobic interactions. The Figure (20-22), and Tables (4-5) illustrate specific interactions, such as H-donor, H-acceptor, and H-pi, along with the distance and energy for each interaction. Molecular docking results show that the standard compounds is the strongest binder to the 8C7Y protein, followed by compound A₁ and then A₄. The standard compound's superiority is due to its formation of a strong, tight network of multiple hydrogen bonds, allowing it to fit perfectly within the active site. While compound A₁ has the second-best binding affinity (-7.86 Kcal/mol, it is distinguished by being the most reliable candidate due to its very loe RMSD valu 0.66 Å. However,

its hydrogen bonds are longer and weaker than those formed by the standard compound, which explaine its lower binding energy. Compound A_4 ranks third with the lowest binding affinity - 7.63 Kcal/mol, as it relies on fewer and weaker interactions compared to the other two compounds. These

results reveal that the protein favors compounds that form short, multiple hydrogen bonds. Practically, A_1 is the best non-standard candidate and couldb be improved to become more effective bt modifying its structure to form stronger bonds.

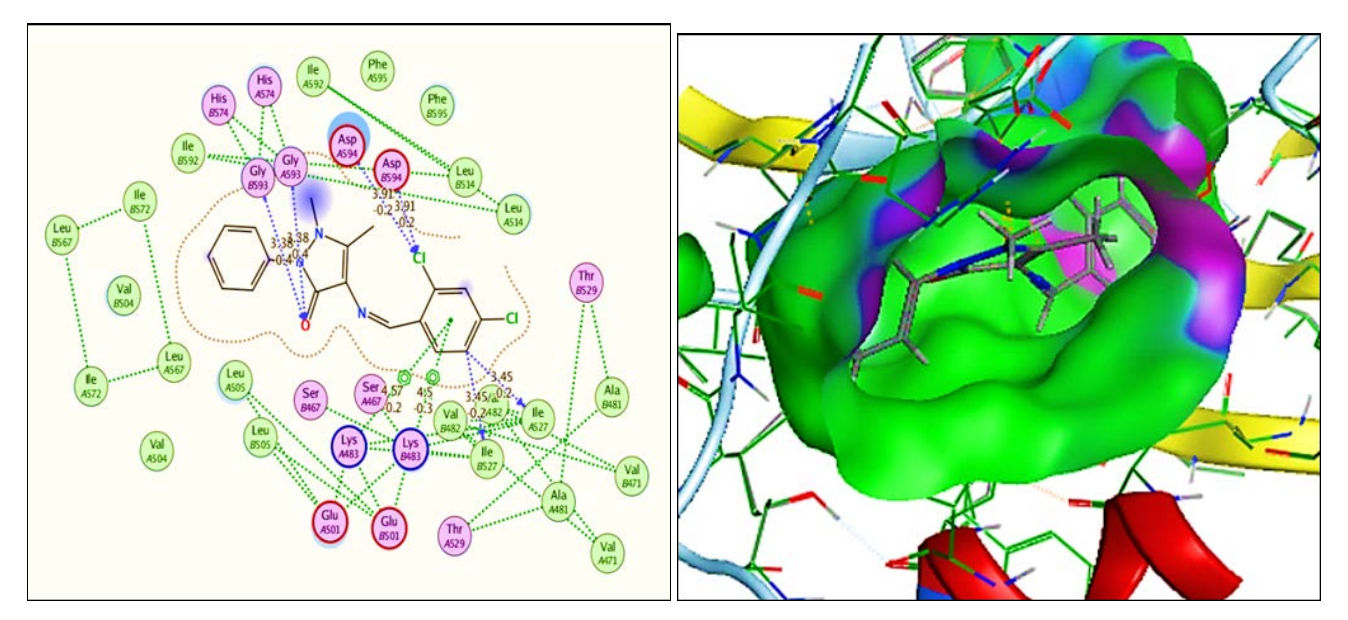


Fig 20: Results an Analysis of Molecular Docking of Compound A₁.

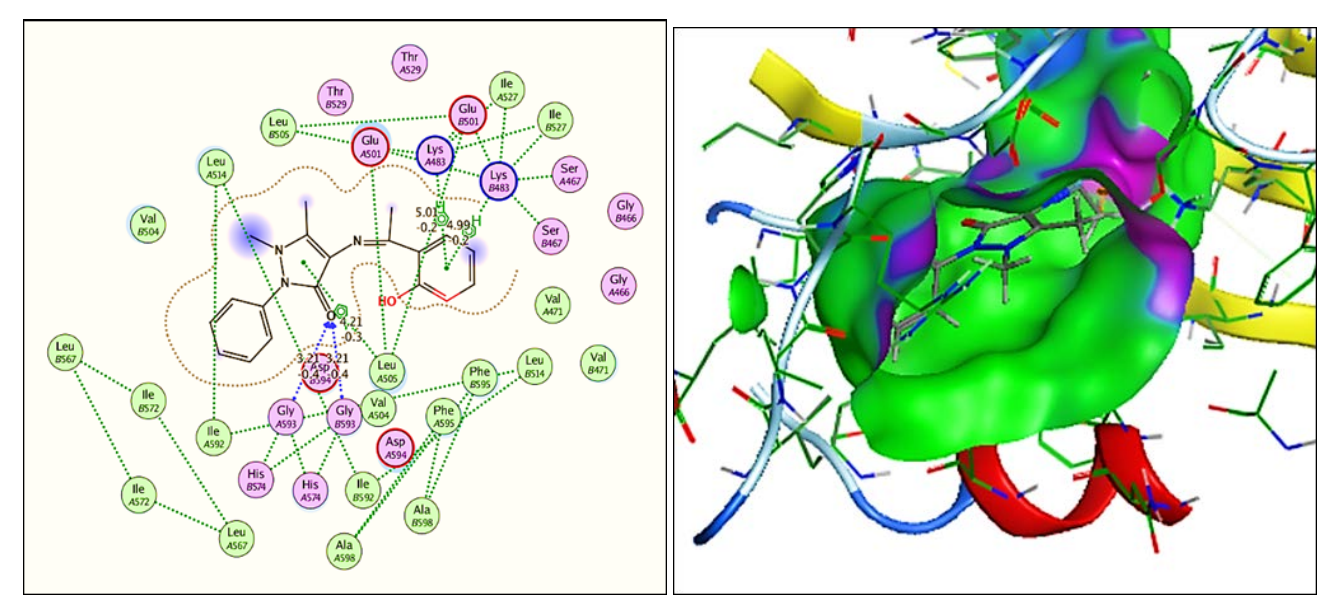


Fig 21: Results an Analysis of Molecular Docking of Compound A4.

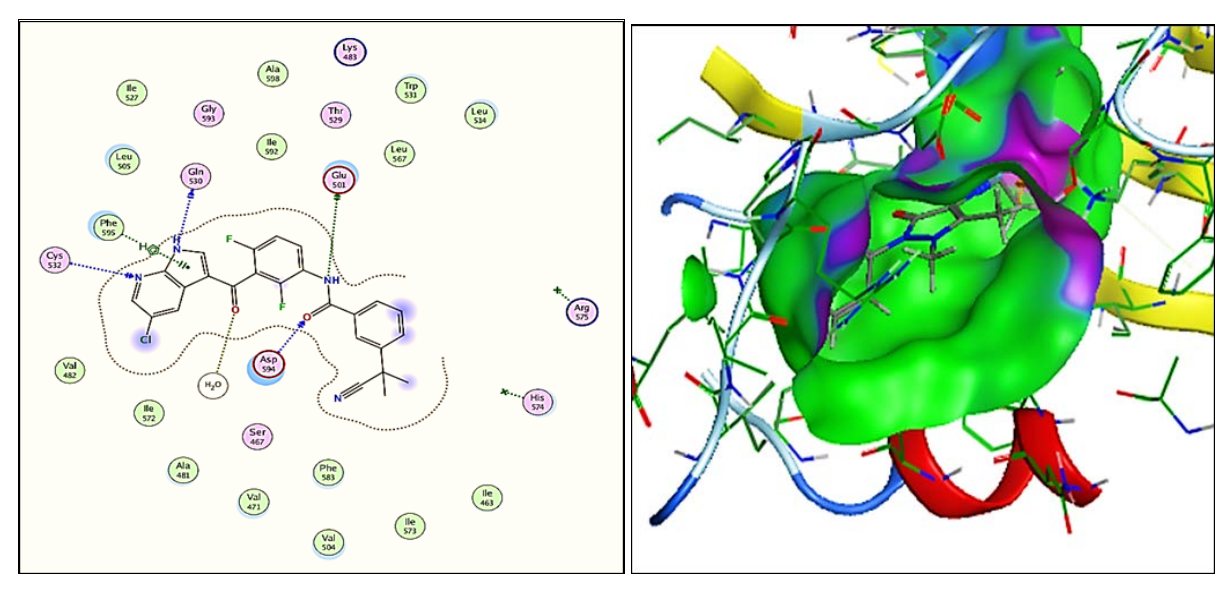


Fig 22: Results an Analysis of Molecular Docking of Compound A₄.

Tabe 4: Molecular Docking Results for Multiple Poeses of Compounds A₁, A₄, and Standard.

Compounds	Binding Affinity Kcal/mol	Rmsd (Å)	Smile
A1-pose1	-7.86467	0.66022	CI
A1-pose2	-7.35383	1.667538	
A1-pose3	-7.29348	1.575044	
A1-pose4	-7.15693	0.847888	CI
A1-pose5	-7.08694	2.615707	N-N
A4-pose1	-7.63144	1.079189	OH
A4-pose2	-7.56244	0.806789	
A4-pose3	-7.54151	0.699183	
A4-pose4	-7.53808	1.604543	•
A4-pose5	-7.5182	1.214126	N-N
standard	-8.62212	1.924656	CI HN N

Table 5: The binding affinity and rmsd result of compounds with 8C7Y.

Compounds No.	The Binding Affinity Kcal/mol	Rmsd (Å)	Atoms of the compound	Receptor Atom	Residues of the involved receptor.	Interaction bond type	Distance (Å)	E (kcal/mol)
			C 21	О	ILE 527	(B) H-donor	3.45	-0.2
			C 21	O	ILE 527	(B) H-donor	3.45	-0.2
			09	CA	GLY 593	(B) H-acceptor	3.38	-0.4
A 11	7.9646	0.66022	O 9	CA	GLY 593	(B) H-acceptor	3.38	-0.4
A1-pose1	-7.8646	0.66022	CL 25	N	ASP 594	(B) H-acceptor	3.91	-0.2
			CL 25 N ASP 594 (B) H-acceptor		3.91	-0.2		
			6-ring	CE	LYS 483	(B) pi-H	4.57	-0.2
			6-ring	CE	LYS 483	(B) pi-H	4.5	-0.3
	-7.6314	1.07918	09	CA	GLY 593	(B) H-acceptor	3.21	-0.4
			09	CA	GLY 593	(B) H-acceptor	3.21	-0.4
A4-pose1			6-ring	CD	LYS 483	(B) pi-H	5.01	-0.2
_			5-ring	CD2	LEU 505	(B) pi-H	4.21	-0.3
			6-ring	CD	LYS 483	(B) pi-H	4.99	-0.2
			N1 1	OE2	GLU 501	(B) H-donor	2.84	-5.5
C4	0.6221	1.02465	N2 6	O	GLN 530	(B) H-donor	2.87	-5.0
Standard	-8.6221	1.92465	O1 10	O	HOH 913	(B) H-acceptor	2.68	-2.4
			N3 16	N	CYS 532	(B) H-acceptor	2.91	-5.3

Comparison of Molecular Docking of Compounds A₁, A₄ and standard with 8C7Y Protein.

This chart (Figure 23), compares the docking performance of compounds A₁, A₄, and the standard ligand with the 8C7Y protein. The blue bars represent the binding affinity, where more negative values indicate stronger binding, while the red line shows the RMSD values, which reflect the stability of the binding poses. From the results, the standard ligand achieves the strongest binding affinity (-8.62 kcal/mol) but with the highest RMSD (1.92 Å), indicating that although it binds most tightly, its pose is less stable.

Compound A₁ demonstrates a slightly weaker binding affinity (-7.86 kcal/mol) but has the lowest RMSD (0.66 Å), making it the most stable and reproducible binding pose. Compound A₄ shows the weakest binding among the three (-7.63 kcal/mol) but still maintains a relatively low RMSD (1.08 Å), suggesting a stable pose with less favorable interactions. Overall, the chart highlights that the standard is the best in binding strength, while A₁ offers the most stable geometry and A₄ provides a consistent but weaker binding interaction.

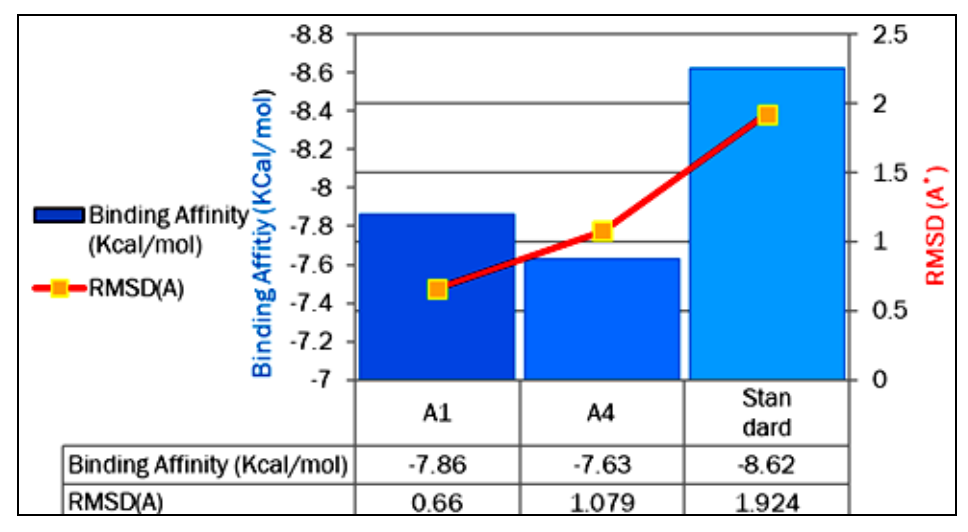


Fig 23: Analysis of Molecular Docking of Compound A₁, A₄ and standard.

DFT Investigation of the Prepared Compounds

All the calculations were performed with Gaussian 09W software with density functional theory (DFT) [33]. Using the B3LYP functional and 3-21G basis set. These calculations included HOMO, LUMO, and several electronic properties [32]. The significance of these computations lies in identifying the most stable and the most reactive compound based on band gap energy ($E_{gap} = E_{LUMO}$ - E_{HOMO}). A smaller energy gap indicates a higher reactivity, while a larger gap corresponds to a more stable compound. This method offers important insights into the electrical structure of the compounds being studied and enables the theoretical prediction of molecular behavior [33]. Higher HOMO energies promote electron donation, whereas lower LUMO energies improve electron uptake. Several equations were used to calculate additional attributes, which are crucial for assessing the stability and activity of the produced compounds [34]. The following formula, $\omega =$ $\mu 2/2\eta$, can be used to calculate the initial parameter, electrophilicity. where (η) is the absolute hardness and (μ) is the absolute electronegativity [35]. The Koopman's theorembased equations (η = (ELUMO - EHOMO)/2, S = 1/ η , and μ = (ELUMO + EHOMO)/2) can be used to calculate these [36]. The HOMO and LUMO energies were used to calculate the electron affinity (A) and ionization energy (I) using the following relationships: A = - EHOMO and I = - ELUMO [37]. The results shown in Table 6 showed that compound A₁ is the most reactive and least stable, while compound A₃ is the least reactive and most stable. This is due to the Egap value for both compounds being 3.352 eV and 4.056 eV, respectively. The excitation of an electron from a HOMO orbital (highest occupied molecular orbital) to a LUMO orbital (lowest unoccupied molecular orbital) depends on

the value of Egap. The lower the Egap value, the easier the excitation of the electron, which increases the compound's ability to react chemically. A compound's capacity to donate electrons is gauged by its HOMO energy [38]. Greater ability to donate electrons is indicated by a higher (less negative) EHOMO value. Contrary to the initial, the date shows that compound A₃ has a less negative E_{HOMO} value (-5.393 eV) compared to compound A₁ (-5.580 eV), making it a better electron donor. Conversely, the LUMO energy (ELUO) reflects a compound's electron-accepting ability. A lower (more negative) E_{LUMO} value signifies a stronger capacity to accept electrons. Compound A₁ has the lowest E_{LUMO} value (- 2.057 eV), confirming it is the best electron acceptor among the series. The stability of these compounds can also be evaluated using the chemical hardness (η) and chemical softness concepts [39]. A high value of (η) corresponds to greater stability and less reactivity. Compound A₁ has the lowest hardness ($\eta = 1.761 \text{ eV}$), reinforcing its status as the most reactive and least stable compound. Conversely, compound A_3 has the highest hardness ($\eta = 2.028$ eV), confirming its superior stability and lower reactivity. Consequently, a compound's softness (the inverse of hardness) increases with its reactivity. Furthermore, the chemical potential (µ) is a key descriptor for evaluating a compound's electronegativity. Compound A₁ has the highest electronegativity potential, which is due to its high electronegativity. Finally, we conclude that compound A₁ is more reactive than other compounds because it has the smallest energy gap and low chemical hardness compared to other compounds. The remaining compounds, A2, A4, and A₅, exhibit intermediate properties in terms of reactivity and stability, placing them between these two extremes, as seen Figure 24.

Table 6: Electronic Properteis (HOMO, LUMO) and other Descirptors of Compounds A1-A5.

	Property (eV)									
Compound No.	E _{HOMO} (eV)	E _{LUMO} (eV)	Egap (eV)	I (eV)	A (eV)	μ (eV)	H (eV)	S (eV)	Ω (eV)	
A_1	-5.580	-2.057	3.523	-5.580	-2.057	-3.818	1.761	0.567	4.138	
A_2	-5.313	-1.412	3.901	-5.313	-1.412	-3.362	1.950	0.512	2.898	
A ₃	-5.393	-1.337	4.056	-5.393	-1.337	-3.365	2.028	0.493	2.791	
A_4	-5.149	-1.162	3.987	-5.149	-1.162	-3.155	1.993	0.501	2.4497	
A ₅	-4.745	-1.140	3.605	-4.745	-1.140	-2.942	1.802	0.554	2.401	

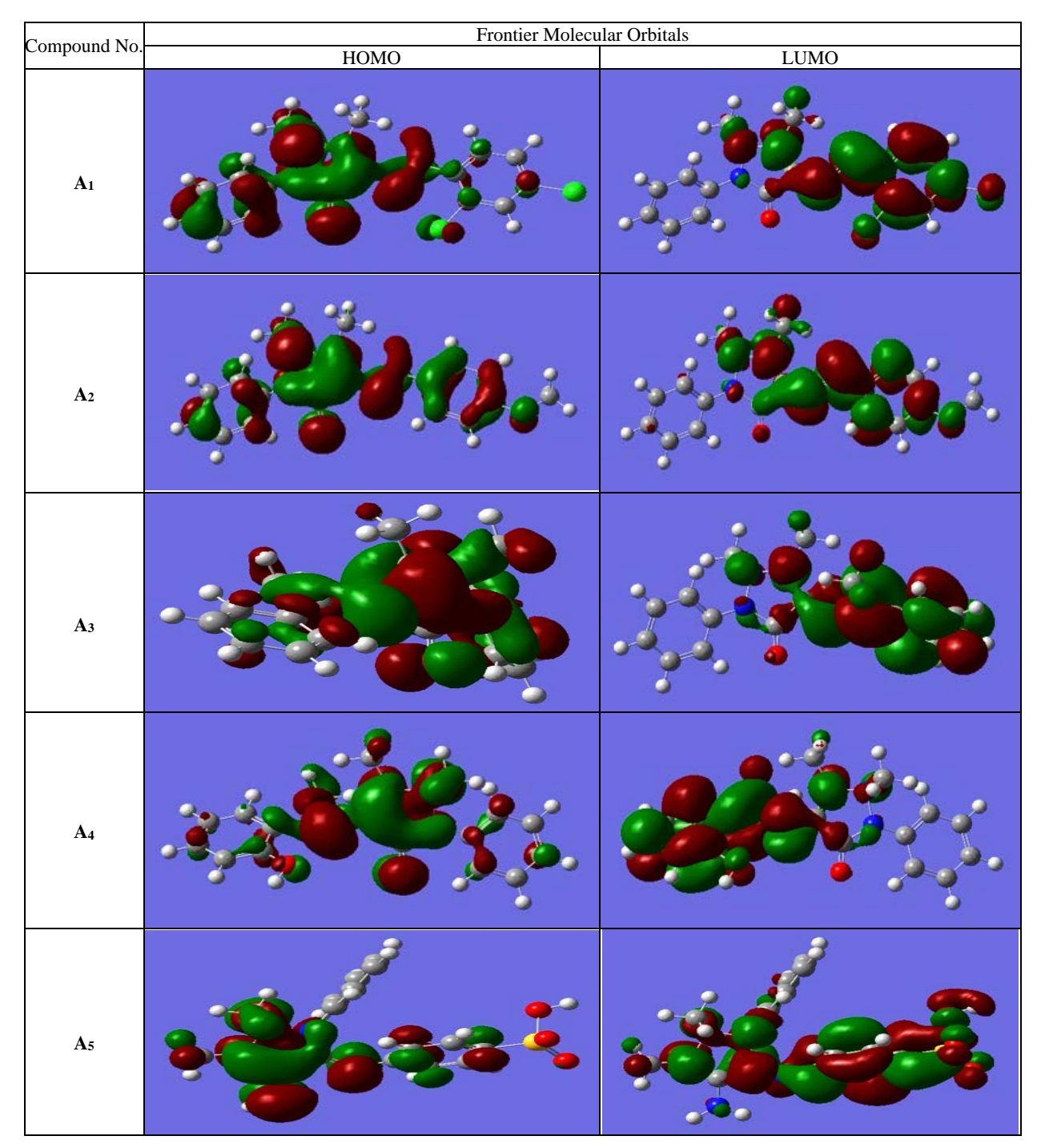


Fig 24: Electron Density Distribution in HOMO and LUMO Orbitals of Compounds A₁-

Mulliken Charge Analysis of Compounds.

The Mulliken charge is a method for calculating the electron density in a molecule and assigning a partial charge to each atom. It's a key tool for understand bond polarity and molecular interactions [40]. From the values shown in Table 7, we can observe the charge distribution across the

compound. Carbon atoms 1, 2, 3, 15, and 16 generally have a large positive partial charge. This indicates that they are bonded to highly electronegative atoms, such as oxygen and nitrogen, which pull electron density away from them, Conversely, carbon atoms at positions 7, 8, and 10 to 14 have a negative partial charge, suggesting they're bonded to

less electronegative atoms or are part of electron-rich regions. As expected, nitrogen and oxygen atoms consistently show negative charges. For example, the nitrogen atoms at positions 4, 5, and 6 exhibit significant negative charges typically ranging from (-0.4) to (-0.8). Similarly, the Oxygen atoms display negative charge of around (-0.5) to (-0.58). These values reflect the high electronegativity of these elements. Hydrogen atoms in all compounds showed a positive charge, ranging from (0.18) to (0.36). This occurs b single electron is patially drawn a way by the more electronegative atome thy're bonded to. A notable observation is in compound A₅, where the sulfur atom (S) at position 22 showed a large positive charge of

(+1.51). This suggests that the sulfur atom has donated a substantial amount of its electron density to its neighboring atoms. A positive charge of (+1.51) was shown for the sulfur atom (22S) of compound A_5 , indicating that it has the ability to donate electron density to nearby atoms. It is also clear that the charge distribution and molecular structure of compounds A_1 - A_4 remain unchanged due to the similarity of the charges on the bonds. By measuring the molecular charge, it is possible to distinguish whether compounds are electron-rich or electron-poor, which enhances our understanding of the behavior of the compound and its interactions with other compounds.

Table 7: Calculated Mulliken Charges for Compounds A₁-A₅

	A ₁		\mathbf{A}_2	A ₃			A ₄₁	\mathbf{A}_{5}		
Atom	Charge	Atom	Charge	Atom	Charge	Atom	Charge	Atom	Charge	
1C	0.715	1C	0.714	1C	0.721	1C	0.723	1C	0.658	
2C	0.045	2C	0.054	2C	0.056	2C	0.052	2C	0.227	
3C	0.410	3C	0.393	3C	0.386	3C	0.376	3C	0.345	
4N	-0.423	4N	-0.416	4N	-0.421	4N	-0.417	4N	-0.419	
5N	-0.627	5N	-0.634	5N	-0.638	5N	-0.642	5N	-0.591	
6N	-0.571	6N	-0.593	6N	-0.636	6N	-0.608	6N	-0.881	
7C	-0.619	7C	-0.617	7C	-0.610	7C	-0.609	7C	-0.609	
8C	-0.413	8C	-0.413	8C	-0.414	8C	-0.413	8C	-0.400	
90	-0.499	90	-0.506	90	-0.508	90	-0.509	9N	-0.722	
10C	-0.201	10C	-0.201	10C	-0.210	10C	-0.202	10C	-0.167	
11C	-0.188	11C	-0.189	11C	-0.189	11C	-0.189	11C	-0.187	
12C	-0.188	12C	-0.189	12C	-0.189	12C	-0.190	12C	-0.172	
13C	-0.189	13C	-0.190	13C	-0.190	13C	-0.190	13C	-0.189	
C14	-0.192	14 C	-0.195	14 C	-0.198	14 C	-0.200	14 C	-0.147	
15C	0.324	15 C	0.329	15 C	0.331	15 C	0.334	15 C	0.245	
C16	0.127	16 C	0.123	16 C	0.314	16 C	0.323	16C	-0.158	
17C	-0.018	17 C	-0.066	17 C	-0.035	17 C	-0.038	17 C	-0.162	
18C	-0.292	18 C	-0.162	18 C	-0.159	18 C	0.316	18 C	0.242	
19C	-0.107	19 C	-0.187	19 C	-0.185	19 C	-0.208	19 C	-0.160	
20C	-0.265	20 C	0.323	20 C	-0.180	20 C	-0.182	20 C	-0.165	
21C	-0.156	21 C	-0.214	21 C	-0.181	21 C	-0.191	21 C	-0.465	
22C	-0.164	22 C	-0.193	22 C	-0.203	22 C	-0.195	22S	1.518	
23H	0.180	23 H	0.173	23 C	-0.616	23 C	-0.617	23O	-0.568	
24Cl	0.116	24 O	-0.548	24 H	0.226	24 O	-0.568	24O	-0.568	
25Cl	0.178	25 C	-0.335	25 H	0.214	25 H	0.224	2 O	-0.586	
26H	0.230	26 H	0.229	26 H	0.222	26 H	0.212	26H	0.296	
27H	0.217	27 H	0.214	27 H	0.238	27 H	0.219	27 H	0.325	
28H	0.227	28 H	0.222	28 H	0.213	28 H	0.235	28 H	0.201	
29H	0.242	29 H	0.237	29 H	0.2111	29 H	0.211	29 H	0.211	
30H	0.217	30 H	0.215	30 H	0.200	30 H	0.209	30 H	0.221	
31H	0.213	31 H	0.209	31 H	0.185	31 H	0.200	31 H	0.214	
32H	0.199	32 H	0.200	32 H	0.182	32 H	0.183	32 H	0.196	
33H	0.186	33 H	0.184	33 H	0.190	33 H	0.180	33 H	0.225	
34H	0.184	34 H	0.182	34 H	0.230	34 H	0.188	34 H	0.197	
35H	0.192	35 H	0.190	35 H	0.224	35 H	0.230	35 H	0.197	
36H	0.229	36 H	0.229	36 H	0.190	36 H	0.177	36 H	0.197	
37H	0.248	37 H	0.226	37 H	0.189	37 H	0.192	37 H	0.198	
38H	0.224	38 H	0.207	38H	0.187	38 H	0.185	38 H	0.209	
39H	0.204	39 H	0.189	39 H	0.184	39 H	0.191	39 H	0.228	
		40 H	0.183	40 H	0.221	40 H	0.218	40 H	0.195	
		41 H	0.225	41 H	0.210	41 H	0.205	41 H	0.197	
		42 H	0.201	42 H	0.226	42 H	0.227	42 H	0.228	
		43 H	0.2007			43 H	0.352	43 H	0.366	

Conclusion

In this work, 4-aminoantipyrine underwent a condensation

reaction with several substituted benzaldehydes, ketones, and sulfonic acid to effectively create a novel family of

Schiff bases. FT-IR, ¹H-NMR, ¹³C-NMR, and mass spectrometry were among the sophisticated spectroscopic methods that conclusively verified the precise chemical structures of the produced compounds. These studies' findings showed that the targeted compounds were produced with a high degree of purity. In particular, mass spectrometry results were crucial for confirming the molecular structures of compounds A1 and A2. Compound A_1 showed a molecular ion peak at m/q = 359.3, which corresponds to the chemical formula [C₁₈H₁₅Cl₂N₃O]. Similarly, compound A2 displayed a molecular ion peak at m/q= 321.3. confirming its chemical formula as [C₁₉H₁₈N₃O₂]. The characteristic fragmentation patterns, along with the base peaks (m/q= 188.1 for A_1 and m/q = 92.8 for A₂). Provided critical information for deducing their full molecular structures. Compounds A₁, A₄, and A₅ were tested for their biological effectiveness against both Gram-positive and Gram-negative bacteria. The outcomes showed how effective these substances are and how much antibacterial activity they have. Notably, A4 displayed high inhibitory activity against Klebsiella and Staphylococcus aureus, with inhibition zone diameteris reaching 26 mm and 22 mm, respectively, at the highest concentration (0.01 mg/ml). Compound A1 also showed strong activity against Enterococcus faecalis, with an inhibition increases with concentration, making them promising candidates for further investigation. In addition, molecular docking studies were performed on compounds A1 and A4 to predict their binding modes with the target protein 8C7Y. The results indicated a good binding energy of -7.86 Kcal/mol compared to A₄ (-7.63 Kcal/mol), which correlates with its higher observed biological activity. This suggests that the biological activity of the compounds is directly related to their ability to form strong hydrogen bonds with the target protein. Finally, DFT calculation were condected to analyze to electronic properties of the synthesized compounds. Compound A₁ was found to have the smallest energy gap (Egap = 3.352eV) and the lowest chemical hardness (η = 1.761 eV). Classifying it as the most reactive and least stable compound. In contrast, compound A₃ was the most stable and least reactive, Possessing the largest energy gap (Egap = 4.056 eV)and the highest chemical hardness ($\eta =$ 2.028 eV) . These theoretical finding provide a strong foundation for understanding the observed experimental results and serve as a guide for designing new, more effective compounds in the future.

References

- 1. Bayrak H, Cebeci YU, Karaoğlu ŞA. Synthesis of novel antipyrine derivatives possessing remarkable antimicrobial activities. ChemistrySelect. 2019;4(44):12906-8.
- 2. Elattar KM, Fadda AA. Chemistry of antipyrine. Synthetic Communications. 2016;46(19):1567-94.
- 3. Fadda AA, Rabie R, Bondock S, Etman HA. Derivational, structural, and biological studies of some new pyrazolyl, isoxazolyl, pyrimidinyl, pyridazinyl, and pyridopyridazinyl from 4-substituted antipyrine. Journal of Heterocyclic Chemistry. 2017;54(2):1304-10
- 4. Ei Ashry E, Awad L, Ibrahim E, Bdeewy OK. Synthesis of antipyrine derivatives derived from dimedone. Chinese Journal of Chemistry. 2007;25(4):570-3.

- Premnath D, Enoch IV, Selvakumar PM, Indiraleka M, Vennila JJ. Design, synthesis, spectral analysis, *in vitro* anticancer evaluation and molecular docking studies of some fluorescent 4-amino-2,3-dimethyl-1-phenyl-3pyrazolin-5-one, ampyrone derivatives. Interdisciplinary Sciences: Computational Life Sciences. 2017;9(1):130-9.
- Gaber M, Elsharkawy M, Bakr EA, Khedr AM. Novel metal chelates with antipyrine tridentate azo dye ligand for antimicrobial and antitumor applications: synthesis, structure affirmation, DFT studies, and molecular docking simulation. Applied Organometallic Chemistry. 2024;38(9):e7632.
- 7. Mnguni MJ, Lemmerer A. A structural study of 4-aminoantipyrine and six of its Schiff base derivatives. Crystal Structure Communications. 2015;71(2):103-9.
- 8. Cunha S, Oliveira SM, Rodrigues Jr MT, Bastos RM, Ferrari J, de Oliveira CM, *et al.* Structural studies of 4-aminoantipyrine derivatives. Journal of Molecular Structure. 2005;752(1-3):32-9.
- 9. Yasar Q, Zaheer Z. 4-Aminoantipyrine analogs as antiinflammatory and antioxidant agents: synthesis, biological evaluation and molecular docking studies. International Journal of Pharmaceutical Investigation. 2021;11(1):1-9.
- Adithya Krishnan M, Saranyaparvathi S, Raksha C, Vrinda B, Girish CG, Kulkarni N, et al. Transition metal complexes of 4-aminoantipyrine derivatives and their antimicrobial applications. Russian Journal of Coordination Chemistry. 2022;48(11):696-724.
- 11. Zúñiga-Miranda J, González-Pastor R, Carrera-Pacheco SE, Rodríguez-Pólit C, Barba-Ostria C, Machado A, *et al.* Experimental and computational studies of Schiff bases derived from 4-aminoantipyrine as potential antibacterial and anticancer agents. Discover Applied Sciences. 2025;7(2):115-26.
- 12. Morens DM, Folkers GK, Fauci AS. The challenge of emerging and re-emerging infectious diseases. Nature. 2004;430(6996):242-9.
- 13. Arumugam A, Shanmugam R, Munusamy S, Muhammad S, Algarni H, Sekar M. Study of the crystal architecture, optoelectronic characteristics, and nonlinear optical properties of 4-aminoantipyrine Schiff bases. ACS Omega. 2023;8(17):15168-80.
- 14. Aguilar-Llanos E, Carrera-Pacheco SE, González-Pastor R, Zúñiga-Miranda J, Rodríguez-Pólit C, Mayorga-Ramos A, *et al.* Crystal structure, Hirshfeld surface analysis, and biological activities of Schiff-base derivatives of 4-aminoantipyrine. ACS Omega. 2023;8(45):42632-46.
- 15. Çakmak R, Başaran E, Boğa M, Erdoğan Ö, Çınar E, Çevik Ö. Schiff base derivatives of 4-aminoantipyrine as promising molecules: synthesis, structural characterization, and biological activities. Russian Journal of Bioorganic Chemistry. 2022;48(2):334-44.
- 16. Hassan AS, Morsy NM, Aboulthana WM, Ragab A. Exploring novel derivatives of isatin-based Schiff bases as multi-target agents: design, synthesis, *in vitro* biological evaluation, and in silico ADMET analysis with molecular modeling simulations. RSC Advances. 2023;13(14):9281-303.
- 17. Al-Tufah M. Synthesis, identification, and biological activity of novel 1,3-oxazepane-7,4-dione compounds. Central Asian Journal of Theoretical and Applied

- Science. 2025:6(1):34-51.
- 18. Al Shammari WA, Lateef SM. Synthesis, structural, thermal and biological studies of ligand derived from anthrone with 4-aminoantipyrine and its metallic complexes. 2022.
- 19. Gerengi H, Cakmak R, Dag B, Solomon MM, Tuysuz HAA, Kaya E. Synthesis and anticorrosion studies of 4-[(2-nitroacetophenonylidene)-amino]-antipyrine on SAE 1012 carbon steel in 15 wt.% HCl solution. Journal of Adhesion Science and Technology. 2020;34(22):2448-66.
- 20. Sherif SH, Kure DA, Moges EA, Argaw B. Synthesis, characterization, and antibacterial activity evaluation of 4-aminoantipyrine derivatives and their transition metal complexes. American Journal of Bioscience and Bioengineering. 2021;9(1):8-12.
- 21. Al-Tufah MM. Synthesis and identification of some new bi-azetidine-2,2'-dione and bi-quinazoline-4,4'-dione compounds derived from bis Schiff base derivatives. Samarra Journal of Pure and Applied Science. 2025;7(2):56-76.
- 22. Demirci S. Synthesis and biological activity studies of some new hybrid compounds derived from antipyrine. Heterocyclic Communications. 2016;22(3):143-9.
- 23. Singh G, Satija P, Singh B, Sinha S, Sehgal R, Sahoo SC. Design, crystal structures and sustainable synthesis of a family of antipyrine derivatives: abolish to bacterial and parasitic infection. Journal of Molecular Structure. 2020:1199:127010.
- 24. Wu J, Zhong QQ, Wang TY, Wang CX, Du Y, Ji S, *et al.* MS-based metabolite analysis of two licorice chalcones in mice plasma, bile, feces, and urine after oral administration. Biomedical Chromatography. 2021;35(3):e4998.
- 25. Walsh TR, Gales AC, Laxminarayan R, Dodd PC. Antimicrobial resistance: addressing a global threat to humanity. Public Library of Science. 2023;19(3):e1004264.
- 26. Al-Tufah MM, Beebaeny S, Jasim SS, Mohammed BL. Synthesis and characterization of ethyl dioxoisoindolinyl cyclohexenone carboxylate derivatives from some chalcones and biological activity assessment. Chemical Methodologies. 2023;7(1):408-18
- 27. Genova-Kalou P, Hikova E, Kereziev T, Kolev P, Mankov V, Veselinov P, *et al.* Does a SPR-based cell-based assay provide reliable results on the toxicity and efficacy of antiviral drugs? Sensors. 2025;25(13):3905-18.
- 28. Prossnitz ER, Barton M. The G protein-coupled oestrogen receptor GPER in health and disease: an update. Nature Reviews Endocrinology. 2023;19(7):407-24.
- 29. Priyanka, Mujwar S, Bharti R, Singh TG, Khatri N. 2,2'-Bipyridine derivatives exert anticancer effects by inducing apoptosis in hepatocellular carcinoma (HepG2) cells. Journal of Hepatocellular Carcinoma. 2024;11:2181-98.
- 30. Ahmad S, Bano N, Raza K. Evaluating the polypharmacological potency of FEDPN from ChEMBL BioAssays against lung cancer EGFR, ALK, TrkA and KRAS proteins. International Journal of Biological Macromolecules. 2025;306:141703.
- 31. Sánchez Rodríguez F, Simpkin AJ, Chojnowski G,

- Keegan RM, Rigden DJ. Using deep-learning predictions reveals a large number of register errors in PDB depositions. IUCrJ. 2024;11(6):938-50.
- 32. Jasm SS, Al-Tufah MM, Hattab AH. Synthesis, spectral characterization, and DFT analysis of novel 3-(4-substituted phenyl)-5-methyloxazolo[5,4-c]isoxazole derivatives. Asian Journal of Chemical Sciences. 2025;15(5):1-30.
- 33. Ergan E. Theoretical studies via DFT calculation of pyrimidine derivatives as potential corrosion inhibitor. Journal of the Institute of Science and Technology. 2021;11(3):2142-51.
- 34. Singh J, Khan MS, Uddin S. A DFT study of vibrational spectra of 5-chlorouracil with molecular structure, HOMO-LUMO, MEPs/ESPs and thermodynamic properties. Polymer Bulletin. 2023;80(3):3055-83.
- 35. Ofem MI, Louis H, Agwupuye JA, Ameuru US, Apebende GC, Gber TE, *et al.* Synthesis, spectral characterization, and theoretical investigation of the photovoltaic properties of (E)-6-(4-(dimethylamino)phenyl)diazenyl-2-octylbenzoisoquinoline-1,3-dione. BMC Chemistry. 2022;16(1):109-22.
- 36. Almodarresiyeh HA, Shahab S, Kaviani S, Sheikhi M, Lopatik DV, Kuvaeva ZI, *et al.* Synthesis, DFT study and bioactivity evaluation of new butanoic acid derivatives as antiviral agents. Biointerface Research in Applied Chemistry. 2022;12(3):3522-39.
- 37. Tegegn DF, Belachew HZ, Salau AO. DFT/TDDFT calculations of geometry optimization, electronic structure and spectral properties of clevudine and telbivudine for treatment of chronic hepatitis B. Scientific Reports. 2024;14(1):8146-57.
- 38. Adole VA. DFT calculations on three 2,3-dihydrobenzofuran-linked chalcones: structural, HOMO-LUMO and spectroscopic (UV-Vis and IR) interpretation. Vietnam Journal of Chemistry. 2023;61(2):147-57.
- 39. Khairul WM, Rahamathullah R, Joni JR, Isa M. Density functional theory (DFT) calculations, synthesis and electronic properties of alkoxylated-chalcone additive in enhancing the performance of CMC-based solid biopolymer electrolyte. International Journal of Hydrogen Energy. 2022;47(65):27866-76.
- 40. Hussein HA, Fadhil GF. Theoretical investigation of para-amino-dichloro chalcone isomers. Part II: a DFT structure-stability study of the FMO and NLO properties. ACS Omega. 2023;8(5):4937-53.